Punyashlok Ahilyadevi Holkar Solapur University

B. Sc. Part II ◆ Semester III

BOTANY

PAPER V

Dr. P. G. Pataskar ◆ Prof. Dr. M. N. Jagtap
Dr. R. S. Suryavanshi ◆ Dr. Mrs. Seema A. Gaikwad
Dr. Vijaya K. Nikam ◆ Dr. Sonali D. Randive

PHADKE PUBLICATIONS

Pune Branch 'Shriphal Prasad', 415, Narayan Peth, Munjaba Lane, Pune - 411 030. • Telefax : (020) 244 82 951.

ISBN 978-93-89343-31-1

Code No. J 382

Price ₹ 50 /-

First Edition as per New Syllabus : September, 2020

➪ **Published by**

Mrs. Neha Mandar Phadke, For Phadke Publications,
1003/4, 'B', 'A' Ward, Ganesha Residency,
Flat No. 8, Shivaji Peth, Kolhapur.

➪ **Printed by**

New Lokpriya Binding Works
B-25, Udyam Co-op., Society, New Industrial Estate,
Y. P. Powar Nagar, Kolhapur - 416 008.

Punyashlok Ahilyadevi Holkar Solapur University

B. Sc. Part II • Semester III

BOTANY

PAPER VI

Dr. P. G. Pataskar • Prof. Dr. M. N. Jagtap
Dr. R. S. Suryavanshi • Dr. Mrs. Seema A. Gaikwad
Dr. Vijaya K. Nikam • Dr. Sonali D. Randive

PHADKE PUBLICATIONS

Pune Branch 'Shriphal Prasad', 415, Narayan Peth, Munjaba Lane,
Pune - 411 030. ♦ Telefax : (020) 244 82 951.

ISBN - 978-93-89343-38-0

Code No. J 385

Price ₹ 30 /-

First Edition as per New Syllabus : September, 2020

➪ **Published by**

Mrs. Neha Mandar Phadke, For Phadke Publications,
1003/4, 'B', 'A' Ward, Ganesha Residency,
Flat No. 8, Shivaji Peth, Kolhapur.

➪ **Printed by**

Shri Prafulla Pathak, at Swaroop Printing Press,
2576/B, Khasbag, Back of Private High School,
Kolhapur - 416 008.

As per Punyashlok Ahilyadevi Holkar Solapur University's Syllabus

B. Sc. Part II

A Hand Book of PRACTICAL BOTANY

PATASKAR • JAGTAP • SURYAVANSHI
NIKAM • GAIKWAD • RANDIVE

PHADKE PUBLICATIONS

Pune Branch 'Shriphal Prasad', 415, Narayan Peth, Munjaba Lane, Pune - 411 030. ■ Telefax : (020) 244 82 951.

ISBN 978-93-86766-21-2

Code No. J 419

Price ₹ 50/-

First Edition as per New Syllabus : October, 2021

• Published by •

Mrs. Neha Mandar Phadke
For Phadke Publications, 1003/4, 'B', 'A' Ward,
Ganesha Residency, Flat No. 8, Shivaji Peth, Kolhapur.

• Printed by •

Shri. Dilip Chougale
Anand Offset Printers,
25 / 3 Y. P. Powar Nagar, Kolhapur - 416 008.

As per Punyashlok Ahilyadevi Holkar Solapur University Syllabus

B. Sc. Part II ◆ Semester IV

BOTANY

PAPER VIII

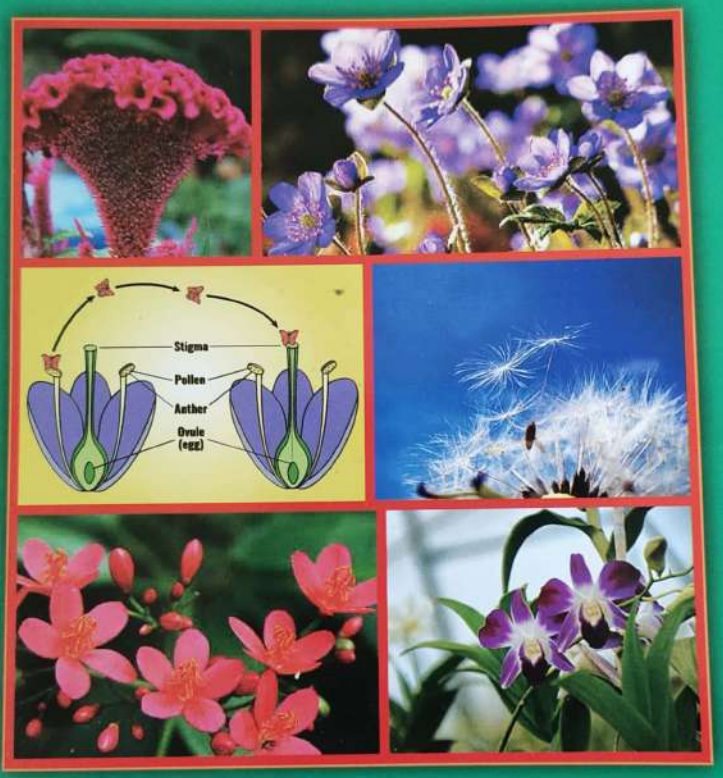

Dr. P. G. Pataskar • Prof. Dr. M. N. Jagtap
Dr. R. S. Suryavanshi • Dr. Mrs. Seema A. Gaikwad
Dr. Vijaya K. Nikam • Dr. Sonali D. Randive

PHADKE PUBLICATIONS

As per Punyashlok Ahilyadevi Holkar Solapur University Syllabus

B. Sc. Part II ◆ Semester IV

BOTANY

PAPER VII

Dr. P. G. Pataskar • Prof. Dr. M. N. Jagtap
Dr. R. S. Suryavanshi • Dr. Mrs. Seema A. Gaikwad
Dr. Vijaya K. Nikam • Dr. Sonali D. Randive

PHADKE PUBLICATIONS

Pune Branch 'Shriphal Prasad', 415, Narayan Peth, Munjaba Lane,
Pune - 411 030. ✦ Telefax : (020) 244 82 951.

ISBN 978-81-952879-7-0

Code No.J408

Price ₹ 30/-

First Edition as per New Syllabus : July, 2021

➪ **Published by**

Mrs. Neha Mandar Phadke, For Phadke Publications,
1003/4, 'B', 'A' Ward, Ganesha Residency,
Flat No. 8, Shivaji Peth, Kolhapur.

➪ **Printed by**

Shri Prafulla Pathak, at Swaroop Printing Press,
2576/B, Khasbag, Back of Private High school,
Kolhapur - 416 008.

Pune Branch 'Shriphal Prasad', 415, Narayan Peth, Munjaba Lane, Pune - 411 030. ◆ Telefax : (020) 244 82 951.

ISBN 978-81-952879-6-3

Code No. J 406

Price ₹ 35 /-

First Edition as per New Syllabus : July , 2021

➪ **Published by**

Mrs. Neha Mandar Phadke, For Phadke Publications,
1003/4, 'B', 'A' Ward, Ganesha Residency,
Flat No. 8, Shivaji Peth, Kolhapur.

➪ **Printed by**

M/s/ Dasharath Book Binding Works,
Yashoda Vishwas Colony,
D. P. Road, Lakshatirth Vasahat, Kolhapur

Punyashlok Ahilyadevi Holkar Solapur University

B. Sc. Part II ◆ Semester IV

As per CBCS Pattern

MATHEMATICS

PAPER VIII

Abstract Algebra

$$e * e' = e$$

$$e * e' = e'$$

$$\phi(aob) = \phi(a) * \phi(b)$$

Jadhav ◆ Mahajan
Gade ◆ Kokare

PHADKE PUBLICATIONS

PUNYASHLOK AHILYADEVI HOLKAR SOLAPUR UNIVERSITY

NEW SYLLABUS

AS PER CHOICE BASED CREDIT SYSTEM (CBCS)

QUALITY TEXT BOOKS

For B. Sc. Part II

Semester IV

CHEMISTRY

Physical Chemistry

NAIK • GURAME

Analytical & Industrial Inorganic Chemistry

BAJAGA • MULIK • VADER

PHYSICS

Paper VII and Paper VIII

PATIL • KOTHAVALE • ZIPARE • KARCHE

MATHEMATICS

Paper VII and Paper VIII

JADHAV • MAHAJAN • GADE • KOKARE

BOTANY

Paper VII and Paper VIII

PATASKAR • JAGTAP • SURYAVANSHI

GAIKWAD • NIKAM • RANDIVE

PRACTICAL BOTANY

PATASKAR ◆ SURYAVANSHI ◆ GAIKWAD

◆ JAGTAP ◆ NIKAM ◆ RANDIVE

PHADKE PUBLICATIONS

Sole Distributors : PHADKE BOOK HOUSE

PHADKE BHAVAN, NEAR HARIMANDIR, DUDHALI, KOLHAPUR - 413 012.

◆ TELEPHONE : (0231)25 40 211 (6 LINES) ◆ MOBILE : 9423508919

◆ Email : customersupport@phadkebooks.in

◆ Website : www.phadkebooks.in

Price ₹ 75 /-

PUNYASHLOK AHILYADEVI HOLKAR
SOLAPUR UNIVERSITY • NEW SYLLABUS

As per CHOICE BASED CREDIT SYSTEM (CBCS)
(introduced from June, 2020)

B. Sc. PART II • SEMESTER IV

MATHEMATICS

(Paper VIII : Abstract Algebra)

by

Dr. B. P. Jadhav
M. Sc., Ph.D. D.H.E
Ex-Head,
Department of Mathematics,
The New College,
Kolhapur.

A. M. Mahajan
M. Sc., SET.
Assistant Professor, Head,
Department of Mathematics
Walchand College of Arts & Science,
Solapur.

Dr. S. P. Gade
M. Sc., NET., Ph.D.
Assistant Professor,
Department of Mathematics,
Sangameshwar College,
Solapur.

B. D. Kokare
M. Sc., B. Ed.
Associate Professor, Head,
Department of Mathematics
Vidnyan Mahavidyalaya,
Sangola.

PHADKE PUBLICATIONS

Distributed by : **PHADKE BOOK HOUSE**

✆ (0231) • 25 40 211 (6 Lines)
• Website - www.phadkebooks.in

Phadke Bhavan,
Near Hari Mandir, Dudhali,
KOLHAPUR - 416 012.

• *E-mail - customersupport @ phadkebooks.in*

Pune Branch 'Shriphal Prasad', 415, Narayan Peth, Munjaba Lane, Pune - 411 030. • Telefax : (020) 244 82 951.

Log on to
www.phadkebooks.in

ISBN 978-93-89343-52-6

Code No.J393

Price ₹ 75/-

First Edition as per New Syllabus : January, 2021

➪ **Published by**
Mrs. Neha Mandar Phadke
For Phadke Publications, Phadke Bhavan,
Near Hari Mandir, Dudhali, KOLHAPUR - 416 012.

➪ **Printed by**
M/s. Dasharath Book Binding Works,
Yashoda Vishwas Colony, D. P. Road,
Lakshatirth Vasahat, Kolhapur

Punyashlok Ahilyadevi Holkar Solapur University

B. Sc. Part II ◆ Semester IV

As per CBCS Pattern

MATHEMATICS

PAPER VII

Differential Equations

$$p^n + P_1 p^{n-1} + P_2 p^{n-2} + ... + P_{n-1}p + P_n = 0$$

$$\frac{dx}{P} = \frac{dy}{Q} = \frac{dz}{R}$$

$$x^n \frac{d^n y}{dx^n} + P_1 x^{n-1} \frac{d^{n-1} y}{dx^{n-1}} + P_2 x^{n-2} \frac{d^{n-2} y}{dx^{n-2}} + ...$$

$$+ P_{n-1} x \frac{dy}{dx} + P_n y = X$$

Jadhav ◆ Mahajan
Gade ◆ Kokare

PHADKE PUBLICATIONS

PUNYASHLOK AHILYADEVI HOLKAR SOLAPUR UNIVERSITY

NEW SYLLABUS

AS PER CHOICE BASED CREDIT SYSTEM (CBCS)

QUALITY TEXT BOOKS

For B. Sc. Part II

Semester IV

CHEMISTRY

Physical Chemistry

NAIK • GURAME

Analytical & Industrial Inorganic Chemistry

BAJAGA • MULIK • VADER

PHYSICS

Paper VII and Paper VIII

PATIL • KOTHAVALE • ZIPARE • KARCHE

MATHEMATICS

Paper VII and Paper VIII

JADHAV • MAHAJAN • GADE • KOKARE

BOTANY

Paper VII and Paper VIII

PATASKAR • JAGTAP • SURYAVANSHI

GAIKWAD • NIKAM • RANDIVE

PRACTICAL BOTANY

PATASKAR ◆ SURYAVANSHI ◆ GAIKWAD

◆ JAGTAP ◆ NIKAM ◆ RANDIVE

PHADKE PUBLICATIONS

Sole Distributors : PHADKE BOOK HOUSE

PHADKE BHAVAN, NEAR HARIMANDIR, DUDHALI, KOLHAPUR - 413 012.

◇ TELEPHONE : (0231)25 40 211 (6 LINES) ◇ MOBILE : 9423508919

◇ Email : customersupport@phadkebooks.in

◇ Website : www.phadkebooks.in

Price ₹ 60 /-

PUNYASHLOK AHILYADEVI HOLKAR
SOLAPUR UNIVERSITY • NEW SYLLABUS

As per CHOICE BASED CREDIT SYSTEM (CBCS)
(introduced from June, 2020)

B. Sc. PART II • SEMESTER IV

MATHEMATICS

(Paper VII : Differential Equations)

by

Dr. B. P. Jadhav
M. Sc., Ph.D. D.H.E
Ex-Head,
Department of Mathematics,
The New College,
Kolhapur.

Prof. A. M. Mahajan
M. Sc., SET.
Assistant Professor, Head,
Department of Mathematics
Walchand College of Arts & Science,
Solapur.

Dr. S. P. Gade
M. Sc., NET., Ph.D.
Assistant Professor,
Department of Mathematics,
Sangameshwar College,
Solapur.

B. D. Kokare
M. Sc., B. Ed.
Associate Professor, Head,
Department of Mathematics
Vidnyan Mahavidyalaya,
Sangola.

PHADKE PUBLICATIONS

Distributed by : **PHADKE BOOK HOUSE**

✆ (0231) • 25 40 211 (6 Lines)
• Website - www.phadkebooks.in

Phadke Bhavan,
Near Hari Mandir, Dudhali,
KOLHAPUR - 416 012.

• *E-mail - customersupport @ phadkebooks.in*

Pune Branch 'Shriphal Prasad', 415, Narayan Peth, Munjaba Lane, Pune - 411 030. • Telefax : (020) 244 82 951.

Log on to
www.phadkebooks.in

ISBN 978-93-89343-51-9

Code No. J392

Price ₹ 60/-

First Edition as per New Syllabus : January, 2021

Published by
Mrs. Neha Mandar Phadke
For Phadke Publications, Phadke Bhavan,
Near Hari Mandir, Dudhali, KOLHAPUR - 416 012.

Printed by
Shri. Dilip Chougale
Anand Offset Printers,
25 / 3 Y. P. Powar Nagar, Kolhapur - 416 008.

आदिवासी साहित्य : संकल्पना, स्वरूप व वाटचाल

संपादक :
प्राचार्य डॉ. शिवलिंग मेनकुदळे
डॉ. पांडुरंग भोसले
डॉ. सचिन रुपनर
डॉ. पौर्णिमा कोल्हे

आदिवासी साहित्य : संकल्पना, स्वरूप व वाटचाल

संपादक

प्राचार्य डॉ. शिवलिंग मेनकुदळे

डॉ. पांडुरंग भोसले

डॉ. सचिन रूपनर

डॉ. पौर्णिमा कोल्हे

AAVISHKAR PUBLICATION

ISBN : 978-81-948864-6-4

आदिवासी साहित्य : संकल्पना, स्वरुप व वाटचाल
Aadivasi Sahitya : Sankalpana, Svarup Va Vatchal

संपादक : प्राचार्य डॉ.शिवलिंग मेनकुदळे, डॉ.पांडुरंग भोसले,
डॉ.सचिन रुपनर, डॉ. पौर्णिमा कोल्हे

भ्रमणध्वनी : ९४२०९७७८२२, ९४२३२५५०३८
ई-मेल : sachinrupnar@gmail.com

प्रकाशक :
सौ.सोनी अहिरे – मोरे
आविष्कार प्रकाशन,
सोमाटणे, तळेगाव दाभाडे, पुणे-४१२१०६
भ्रमणध्वनी : ९९६०१६९९७४, ८३९००४७१७४
ई-मेल : aavishkarprakashan@gmail.com

अक्षरजुळणी/मुद्रक :
श्री. मनोज घोडके, श्री. दीपक मोरे
भ्रमणध्वनी : ८३९००४७१७४, ९९६०१६९९७४

मुखपृष्ठ : श्रीराम रसाळ

प्रथमावृत्ती : ५ सप्टेंबर २०२१

मूल्य : रू. ४९०/-

---

* या पुस्तकात समाविष्ट असलेल्या लेखातील मतांशी संपादक मंडळ सहमत असेलच असे नाही.

अनुक्रमणिका

५०.

नागा जमातीचे सामाजिक व सांस्कृतिक जीवन

डॉ. रघुनाथ फुले, सांगोला

पृथ्वीला आपण बहुरत्ना वसुंधरा म्हणतो. पृथ्वी हेच मानवाचे घरकुल आहे. पृथ्वीवरील सजिवांची निर्मिती हीच निसर्गाची मोलाची देणगी आहे. सर्व सजिवांमध्ये मानव हा सर्वश्रेष्ठ बुद्धिमान प्राणी आहे. मानव जंगलांमध्ये, जलाशयाजवळ वास्तव्य करीत असलेला दिसून येतो. प्राचीन काळी मानव हा निसर्गाचा दास होता. मानव (ख्रिस्तपूर्व वीस हजार वर्षापूर्वी) गुहेमध्ये किंवा झाडाच्या डोलीमध्ये रहात होता. शिकार, कंदमुळे, फळे गोळा करुन आपला चरितार्थ चालवित असे. सुरुवातीला अगदी रानटी मागासलेल्या अवस्थेत जीवन जगत होता. त्या काळात दगड हेच त्याचे मुख्य हत्यार होते. सुरुवातीला नैसर्गिक आपत्तींना निसर्गाची शक्ती मानून देव मानत होता.

मानवामध्ये जसजशी प्रगती होत गेली, तसतसे मानवाच्या राहणीमानामध्ये बदल व विकास होत गेला. परंतु आजही जगात आदिम जमाती पहावयास मिळतात. थंड हवामानातील एस्किमो, उष्ण प्रदेशातील पिग्मी, बुशमेन भारतातील गोंड, भिल्ल, संथाल, नागा, कातकरी, बोडो, खोंड, लोम्बडी, सावरा, आंदमानी, गारो, निकोबारी, ओग, जारवा, ओंजल, खासी इत्यादी मुख्य जमाती आढळतात.

नागा ही ईशान्य भारतातील प्रमुख वैशिष्ट्यपूर्ण आदिवासी जमात आहे. याचकारणाने नव अभ्यासकांचे या जमातीकडे लक्ष वेधले गेले आहे. या जगात या जमातीच्या अनेक लहान-मोठ्या उपजमाती आहेत. चंग, फोम, लोथा, सेमा नागा या प्रसिद्ध आहेत. 'नागा' या शब्दाच्या उत्पत्तीविषयी वेगवेगळी मते आहेत. काहींच्या मते 'नागा' हा शब्द संस्कृतमधील 'नग' या शब्दापासून बनलेला असावा. 'नग'चा अर्थ पर्वत असा होतो. काहींच्या मते नागा हा शब्द संस्कृतमधील नग्न या शब्दापासून बनलेला आहे. नागा लोक सापाचे पूजक असल्याने त्यांना 'नागा' हे नाव देण्यात आले आहे. नागा लोक पर्वतावर राहतात.

स्वातंत्र्यपूर्व काळात इंग्रजांच्या शासनव्यवस्थेमुळे व ख्रिश्चन पाद्र्यांच्या

धर्मप्रसारामुळे पाश्चात्य संस्कृतीचा त्यांच्यावर परिणाम झालेला आहे. नागालँड या राज्याची निर्मिती ८ फेब्रुवारी, १९६१ रोजी झाली. या राज्यात नागा लोकांची संख्या अधिक प्रमाणात दिसून येते.

आजही नागा जमात जंगलात, डोंगराळ भागात रहात आहे. त्यांचे जीवन मागासलेले व कष्टप्रद, एकाकी आहे. त्यांची आजही वेगळी संस्कृती टिकून आहे. नागा जमात तशी मंगोलॉइड वंशाची असून ते सुरुवातीपासून ईशान्य भारतात रहात असल्यामुळे त्यांचा वंश इंडो-मंगोलॉइड या नावाने ओळखला जातो. नागा जमातीच्या भाषा भिन्न-भिन्न आहेत. त्यांची मूळ भाषा ही तिबेटी व ब्रह्मी या भाषांच्या मिश्रणातून आलेली असावी. मात्र त्यांच्या भिन्न-भिन्न जमातींमध्ये प्रचलित असलेल्या भाषा वेगवेगळ्या आहेत. एका जमातीची बोलीभाषा दुसऱ्या जमातीस समजू शकत नाही असे दिसून येते.

डॉ. गुहा यांच्या मते नागा लोकांच्या शरीररचनेवरून हे लोक मंगोल वंशाचे असून काही नागा लोक देखणे, उंच, गव्हाळ वर्णाचे व सदृढ आहेत. त्यांचे कपाळ रुंद, डोळे घारे व बारीक, दृष्टी भेदक, नाक बसके आहे. नागा स्त्रिया सुस्वरूप, लठ्ठ, ठेंगण्या तर काही कुरूप असलेल्या दिसतात. नागा लोकांचे स्वभाव उग्र, हिंसक व क्रुर आहेत. नागा लोक शत्रूला कधीही भीत नाहीत, परंतु जागरूक राहतात.

नागा लोकांचे सामाजिक व सांस्कृतिक जीवन इतर आदिवासी समाजापेक्षा वैशिष्ट्यपूर्ण आहे. नागा जमातीत प्रतिष्ठेला खूप महत्त्व आहे. पूर्वी हे लोक माणसाची शिकार करीत असत. शत्रूला ठार मारून त्याचे डोके घरी घेऊन येत असत. ज्याच्या घरामध्ये माणसाच्या कवट्या जास्त तो प्रतिष्ठित समजला जात असे. परंतु ब्रिटिशांनी यावर बंदी आणली आणि ही प्रथा बंद केली.

हे लोक दुर्गम भागांमध्ये राहत असल्याने त्यांचे जीवन कष्टप्रद असलेले दिसून येते. अलिकडे डोंगरउतरणीवर पायऱ्यापायऱ्याची शेती व पशुपालन करून आपले जीवन जगताना दिसतात.

नागा लोकांच्या काही उपजाती स्वतंत्र वृत्तीच्या आहेत. त्यांना इतरांची सत्ता सहन होत नाही. नागा हे निश्चयी, करारी, आनंदी व उत्साही असलेले दिसतात. सर्वसामान्य नागा हे साधे, प्रामाणिक, निष्पाप व सत्यवादी असून ते सौंदर्यप्रिय आहेत. त्यांना नृत्य, संगीत, कला यांची आवड आहे. त्याचबरोबर

ते शौर्य, धैर्य, बुद्धिमान, चपळ, शिस्तप्रिय, कष्टाळू व आदरातिथ्य करणारे आहेत. समाजनियमांचे कसोशीने पालन करताना आढळतात. एखाद्याने जर समाजविरोधी कृत्य केले तर त्याला कठोर शिक्षा दिली जाते. त्यामुळे सामुदायिक जीवन सहकार्याने जगतात.

पूर्वी नागा वस्तीत कुमारगृहे होती, त्यास 'मोरुंग'असे म्हणतात. 'मोरुंग'ला सामाजिक महत्त्व होते. एकाच वयाची मुले व मुली या कुमारगृहाचे सदस्य असतात. त्या कुमारगृहात सांस्कृतिक कार्यक्रम होतात. त्यांचे प्रत्येक कुमारगृह म्हणजे विद्यालय, क्रीडामंडळ, विविध प्रकारच्या शिक्षणाचे केंद्र; विचार विनिमयाचे प्रमुख ठिकाण असलेले दिसते. ते विशिष्ट नियमांनी बांधलेले असून त्या नियमांचे काटेकोर पालन करणे बंधनकारक असते. त्या नियमांचे योग्य पालन केले जाते की नाही ते पाहण्यासाठी तेथे अधिकारी असलेला दिसतो. मुला-मुलींवर सतत देखरेख ठेवली जाते. यामध्ये सामाजिक व सांस्कृतिक परंपरा समजावून दिली जाते. या गृहांना वेगवेगळी नावे आढळतात. कोन्याक युवागृहाना 'मोरुंग' तरूण तरुणींच्या युवागृहाना 'पो' म्हणतात.' 'आओ' व 'अंगामी' नागा यांच्या युवागृहाना अनुक्रमे 'अरिची' व 'किंचुकी' म्हणतात.

युवागृहामध्ये सहकार्य व सद्भावाची भावना दिसते. यात शेती, शिकार, सण, उत्सव यांच्याबद्दल माहिती दिली जाते. कोणताही सामाजिक व सांस्कृतिक कार्यक्रम पार पाडण्यासाठी युवागृहातील मुला-मुलींचा फार मोठा वाटा असतो. ही मुले-मुली समाजातील गरीब बांधवाना शेतातील कामासाठी मदत करतात. कोणाचेही काम अडून रहात नाही. एकूणच काय ही युवागृहे त्या गावाची एक प्रकारची शक्तीच असतात.

नागा जमातीमध्ये पितृसत्ताक कुटुंबपद्धती अस्तित्वात आहे. विभक्त कुटुंब-पद्धतीही रूढ असलेली दिसते. विवाह झाल्यानंतर मुलगा वेगळा राहतो. त्यामध्ये स्त्रियांना मानाचे स्थान असते.

मुले-मुली वयात आल्यानंतर विवाह करतात. बहुतांशी तरुण-तरुणी स्वतःच आपला जोडीदार निवडून विवाह करतात. आईवडिलांची संमती घेऊन ते एकत्र राहतात. नागा जमातीमध्ये 'वधूमूल्य' देण्याची प्रथा आहे. जर एखाद्या वराला 'वधुमूल्य' देण्याची ऐपत नसेल तर त्याला वधूच्या वडिलांच्या घरी काम करावे लागते. नागा जमातीमध्ये बहिर्विवाह पद्धती प्रचलित आहे. यात आपल्या

गोत्रातील मुलींशी विवाह करण्याची प्रथा नाही. जर कोणी प्रयत्न केला तर त्याला शिक्षा भोगावी लागते. या समाजात स्त्रियांची संख्या कमी असल्याने 'अपहरण विवाह' अद्यापही प्रचलित आहे. विवाहित स्त्रीच्या वर्तनावर नागा लोकांचे कडक निर्बंध आहेत. अनैतिक वर्तनाच्या पुराव्यावरून स्त्रीला घटस्फोट देण्यात येतो. याबरोबरच गुन्हेगाराला मंडळाकडून कडक शिक्षा दिली जाते.

नागा लोकांचे प्रेम झाकून ठेवले जात नाही. नागा तरुण प्रथमच एखाद्या मुलीवर प्रेम करीत असेल तर तो आपल्या काळ्या कपड्यात कवड्यांच्या तीन हारी बांधतो. त्यांचा प्रेमसंबंध वाईट समजत नाहीत. नागा कुटुंबात मुलगी वयात आल्यानंतर तिच्यासाठी दाराच्या बाहेर एक वेगळी खोली बांधून दिली जाते. या खोलीत तिला भेटण्यासाठी गावातील तिचे प्रेमिक व दुसऱ्या गावातील तिचे प्रेमिक येतात.

नागा जमातीत विवाहप्रसंगी नाच-गाणी, खाणे-पिणे यांना फारच प्राधान्य असते. नागा तरुणाचे लग्न झाल्यानंतर तो वेगळे राहू शकतो परंतु संपत्तीमध्ये वाटा मिळत नाही. वडील वारल्यानंतर थोरला मुलगा घर सांभाळतो. अविवाहित भाऊ थोरल्या भावाबरोबर राहतात. शेती, घरबांधणी, हस्तकला, घरातील कामे इ.मध्ये स्त्री-पुरुषांना सहकार्य करतात. नागा स्त्रियांचा दर्जा कुटुंबात उच्च असतो. ते सुखी व असेल त्यात समाधानी जीवन जगतात. नवरा बायको यांचा दर्जा हा सारखाच असलेला दिसतो. नागा स्त्रियांना गोंदून घेण्याची हौस असलेली दिसून येते. पूर्वी गोंदून घेतल्याशिवाय विवाह होत नसे.

पूर्वी नागा लोकांमध्ये वेगवेगळी समाजव्यवस्था होती. अंगामी नागांमध्ये प्रजातन्तरात्मक पद्धती होती. प्रत्येक व्यक्तीला स्वातंत्र्य होते. अंगामी नागा वस्तीत एक प्रमुख व्यक्ती असे त्या प्रमुख व्यक्तीस ते 'टेपो' म्हणत असत. त्यांना धार्मिक अधिकार होते, तर कोन्याक नागात सरंजामशाही पद्धत होती. या पद्धतीत गावाची व्यवस्था एका सरदाराकडे असे. हा सरदार गावाचा शासक असे.

नागा लोक रसिक दिसतात. त्यांना नाच-गाण्याची प्रचंड आवड असलेली दिसून येते. त्यांच्या बोलीभाषांमध्ये असंख्य लोकगीते असून तरुण-तरुणी समरस होऊन नृत्य करतात. नृत्यात भाग घेणारे सर्व लोक डाओ, भाले, ढाली इ. शस्त्रांनी व सुंदर शिरस्त्राने घालून स्वतःला सजवतात. त्या शिरस्त्रानाला

बकरीचे केस व पिसे लावून सजवितात. तसेच मण्याच्या माळा, हस्तिदंत किंवा लाकडी कडी इत्यादी दागिने अंगावर घालतात. निरनिराळ्या रंगाची भडक कपडे किंवा काळ्या रंगाचे वस्त्र कंबरेभोवती गुंडाळतात.

नागा लोकांमध्ये प्रत्येक गावाचा कारभार स्वतंत्रपणे चालतो. प्रत्येक जमातीचे मंडळ असते. हंगामी, लोथा, रेंगमा वगैरे जमातीच्या ग्राम संस्थेत गावातील सर्वच वयस्क भाग घेतात.

नागा लोकांचे नवीन वर्ष मे महिन्यामध्ये सुरू होते. वर्षाचा शुभारंभ 'मोत्सू' नृत्याने करतात. त्या वेळी गावाची साफसफाई केली जाते. नृत्यवेश, अलंकार व आयुधे स्वच्छ करतात. या उत्सवात तरुण-तरुणी खूप मद्यपान व बेहोषपणे नाचतात. या उत्सवात स्वैर वर्तनाला मुभा असते. भाताची कापणी झाल्यानंतर 'पोकपटूगी' उत्सव साजरा करतात. विशिष्ट खेळ खेळतात. एकंदरीतच नागा जमातीचे सामाजिक व सांस्कृतिक जीवन वैशिष्ट्यपूर्ण असल्याचे प्रत्ययाला येते.

संदर्भग्रंथ :

१. खतीब, के.ए., ''मानवी भूगोल'', मेहता पब्लिशिंग हाऊस, पुणे, २००६.
२. सवदी, ए.बी., कोळेकर, पी.एस., ''मानवी साधन संपत्ती भूगोल'', निराली प्रकाशन, पुणे, २००९.
३. सावंत, (डॉ.) प्रकाश, ''मानवी भूगोल'', फडके प्रकाशन, कोल्हापूर, २००९.

***

International e-Conference on Recent Trends in Nano-Materials and Its Applications-2021
In Association withInternational Journal of Scientific Research in Science and Technology
Volume 9 | Issue 2 | Print ISSN: 2395-6011 | Online ISSN: 2395-602X (www.ijsrst.com)

Electrochemical Synthesis of Vanadium Oxide Thin Films for Super Capacitor Application : A Review

R. S. Gaikwad[1], S. S. Dhasade[1], S. B. Patwari[2], P. M. Kharade[3], S. D. Patil[4],
J. V. Thombare[1*]

[1]Vidnyan Mahavidyalaya, Sangola, Tal-Sangola, Dist-Solapur, Maharashtra-413307, India
[2]Lal Bahadhur Shastri Mahavidyalaya, Dharmabad-431809, Maharashtra, India
[3]Shankarrao Mohite Mahavidyalaya, Akluj, Dist-Solapur, Maharashtra, India
[4]Pratapsinh Mohite Mahavidyalaya, Karmala, Dist-Solapur, Maharashtra, India

ABSTRACT

The Electrodeposition of Vanadium oxide (VO) thin films are of great interest because of numerous applications in the field of electrochemical devices. Varieties of chemical and physical methods are available for synthesis of VO thin films. In the present mini review we are focusing on the synthesis of VO thin films by Electrodeposition methods and properties. We have studied the comparative study of structural and morphological properties of VO thin films. As per literature it is evident that as deposited VO thin films are amorphous in nature while upon annealing treatment VO thin films changes to crystalline nature. As deposited VO thin films have showed smooth nature but upon in-situ or ex-situ treatments morphology of VO thin films changes to nanostructures, nanoplates, inverse opal like structures etc. Also, we tried to compare the supercapacitive study of electrochemically deposited VO thin films.

Keywords: Electrodeposition, Vanadium Oxide, Thin Films, Supercapacitive Study, etc.

I. INTRODUCTION

Recently, researchers are trying to find the easy way for synthesis of thin films for suitable applications. Generally, the thin films are prepared by some physical methods and lots of thin films are prepared by chemical methods. The physical methods requires sophisticated instruments for preparation of thin films, also they require some ideal conditions such as pressure inside the instrument, vacuum, particular environment, temperature etc. So, these things waste time and other efforts. Other methods are chemical methods such as chemical bath deposition, Successive Ionic Adsorption and Reaction (SILAR) method, Electrodeposition, Sol-Gel method, Co-precipitation method, Solid State Reaction method etc. These methods have some advantages such as they do not require highly sophisticated instruments, precursors for synthesis easily available, not necessary to achieve ideal condition etc. But amongst of all chemical methods Electrodeposition is a unique chemical method for synthesis of various methods and deposited films have various applications such as supercapacitor, gas sensor, solar cell etc.

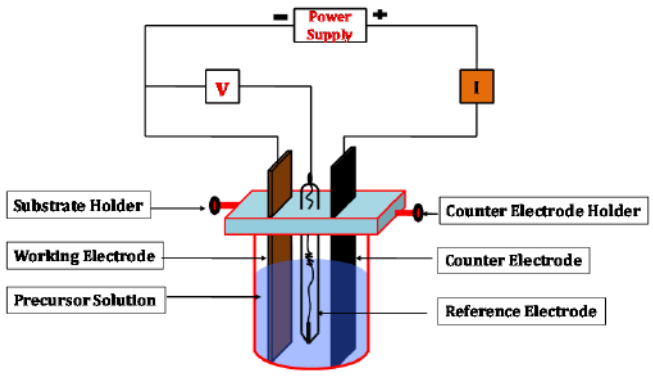

Figure 1: Schematic representation of Electrodeposition process having three electrode configurations.

In case of Electrodeposition, the depositing system consists of a deposition bath, three or two electrodes i.e. working electrode, counter electrode and reference electrode, and a power supply which provide electric field. Sometime, Electrodeposition process is mentioned as electrochemical process because materials are deposited from liquid phase (in deposition bath) to solid phase (on working electrode) by application of proper electric field. In Electrochemical synthesis, each component has its special role for making chemical change in material. Fig 1 shows the schematic presentation of Electrodeposition process.

As per requirement, researchers have made some modifications in the basic structure of Electrodeposition. There may be modification in bath such as making complex in the solution instead of just source solution. Also, there may be modification in bath temperature (i.e. at various temperatures), etc. So, Electrodeposition has variety of parameters through which we can get the proper thin film of suitable properties.

Many researchers have taken efforts to synthesis metal oxide thin films by Electrodeposition method such as NiO [1], Cu_2O [2], ZnO [3-4], molybdenum oxide [5], Manganese and Molybdenum Mixed Oxide [6], Cerium Oxide [7], ruthenium oxide [8], Vanadium Oxide/Manganese Oxide Hybrid [9] etc. Basically, electrochemical synthesis is preparing metal oxide based thin films at room temperature or as deposited films are not in oxide forms. So for proper phase or metal oxides post deposition treatments are necessary, such as annealing, sintering etc.

In the literature, we found that the VO thin films have been formed by various methods such as sol gel method [10], sputtering method [11], spray pyrolysis method [12], electron beam evaporation method [13], vacuum evaporation method [14], electrodeposition method [15], hydrothermal synthesis method [16], etc. In this review, we are focusing on the aspect of electrochemically synthesized VO thin films. Because it has some advantages over other methods, such as this method can be extended to industrial scale, even at low temperature ease of synthesis, this method is non-toxic i.e. environmentally friendly and the deposition set up requires low cost etc.

II. RESULTS AND DISCUSSIONS

A) Electrochemical synthesis of VO thin films:

The VO thin films can be electrodeposited by three different modes such as potentiostatic mode (by keeping constant applied potential across working and counter electrode), galvanostatic mode (by keeping constant applied current density across working and counter electrode) and potentiodynamic mode (by varying potentials across working and counter electrode). In the Electrodeposition of VO thin films, it is evident that every parameter is important to control the film quality. Here it is found that deposition mode, precursors and its concentrations, electrolyte either aqueous or non-aqueous, working electrode i.e. substrate, deposition time or deposition cycles etc., these parameters are very important to study the Electrodeposition of VO thin films. Here we have summarized few reports for Electrodeposition of VO thin films in Table 1.

Table 1: Electrodeposition of VO thin films

Sr. No.	Mode of deposition	Parameters	Precursors	Substrate	Reference
01	potentiodynamic	from +0.2 to -0.7 V (SCE) at 50 mV/s for several hours	NH_4VO_3	150 stainless steel mesh	[17]
02	Galvanostatic	current density of 10-12 mA/cm^2	oxovanadium sulfate solutions (0.2 mole/L, pH 1.8-2.0)	stainless steel 18H12X9T plates	[18]
03	Potentiostatic	2.5 volt for 5 min	0.05 M NH_4VO_3 aqueous solution	ITO-coated glass substrate	[19]
04	Potentiostatic	2 V vs SCE	0.25 M $VOSO_4.xH_2O$ solution in 1:1 (v/v) mixture of deionized water and ethanol	ITO/FTO coated glass	[20]
05	Potentiostatic	0.7 V vs. SCE	0.1 M $VOSO_4$	a piece of carbon cloth	[21]
06	potentiodynamic	the potential 20 times between 0 mV and 2000 mV at a rate of 50 mV/s	50 mM $VOSO_4.H_2O$ solution dissolved in 1.0 M H_3PO_4	PtIr wire	[22]
07	Galvanostatic	3 mA cm^{-2} for 1800 s	1 M aqueous Vanadium sulfate oxide hydrate solution containing 50% wt. ethanol	polystyrene sphere (PS) template	[23]

B) Structural study:

The electrodeposited vanadium oxide thin films have been characterized by x-ray diffraction (XRD) study. From the literature, it is found that the deposited films are in amorphous nature. After annealing, electrodeposited vanadium oxide film becomes crystalline in nature. Ghosh and et al have been reported that the deposited V_2O_5 samples annealed at 200 °C under ambient conditions show no characteristic peak ambient condition of V_2O_5 and after annealing at 500 °C reveals polycrystalline nature of V_2O_5 samples [24]. Raj and et al have reported the calcinations of vanadium oxide thin films for better crystallinity. They have reported the orthorhombic phase with the lattice parameters of a=11.54Å, b=4.383Å and c=3.571Å. The calculated value of crystallite size was reported to be 18 nm [25]. Tsui and et al have reported the partial reduction of V_2O_5 by annealing in air. According to their study, it is evident that the as deposited films are amorphous in nature while upon annealing the films showed monoclinic crystalline structure, possibly intermixed with nanocrystalline/amorphous phases [26]. Yu and et al have been reported that as deposited vanadium

oxide thin films are hydrated in nature and growth is along (001) direction, upon annealing at 500 °C vanadium oxide thin films were completely dehydrated and transforming to orthorhombic phase. Also, after annealing crystallite size changes from 4.2 nm to 32.1 nm and interlayer distance changes from 10.94 A° to 4.23 A° [27]. Aamir and et al have reported XRD pattern of the sample annealed at 350 °C for 4 h. They have reported orthorhombic V_2O_5 having two layers comprising of stacks of distorted VO_5 square pyramids that share edges forming zigzag double chains [28]. Le and et al have reported α and β two phases V_2O_5 films [29].

C) Morphological study:

The morphological study provides the basic structure of materials, also with the help of morphological study it's easy to correlate with other study for analysis of results. The morphological study is made with the help of SEM images.

Aamir and et al have reported the compact and agglomerated V_2O_5 with no specific morphology as they undergo irregular growth with larger particles by potentiostatic mode of electrodeposition. Also, they have reported that formation of well-defined nanoplates like morphology having particle size 200–300 nm with voids prepared by Galvanostatic mode of electrodeposition. So, here we found that the deposition method alters the morphology of vanadium oxide films [28]. The post deposition treatments such as annealing also have influence on the morphology of vanadium oxide thin films. Le and et al have reported the effect of annealing temperature on morphology of vanadium oxide thin films. They have reported that as deposited vanadium oxide thin films shows smooth surface due to amorphous nature and upon annealing at 500 °C or above temperatures the nanorods are formed and as annealing temperature increase the length of nanorods increases this is may be attributed to the high diffusion rate in the surface of the film [29]. Some researchers have tried to control the morphology of vanadium oxide films during electrodeposition, like use of template. Armstrong and et al have reported the use of opal template for control of morphology of vanadium oxide thin films. They have reported that morphology without opal template is undulating film-like structure, while with the help of opal template it becomes inverse opal like structure [20]. In case of electrodeposition, various parameters can be controlled for getting particular morphology, such as electrodeposition time. Lu and et al have reported that electrodeposition time increased from 40 seconds to 60 seconds, the morphology changed from smooth to typical sea-island like morphology [30]. Lu and Zhou have reported the combination of in-situ and ex-situ treatment on vanadium oxide thin films and they have been reported that morphology of vanadium oxide thin films without in-situ or ex-situ or both treatments are featureless. They have found that upon in-situ and ex-situ treatment, morphology changes from non porous nano-particles to nano-rods [31]. All these reports are summarized in Table2.

Table2: Effect of in-situ and ex-situ treatments for electrodeposition and its effect on morphology

Sr. No.	Effect	Morphology	Reference
01	By changing mode of electrodeposition	No specific morphology to well defined nanoplates	[28]
02	By increasing annealing temperature	Smooth surface to nano-rods with increasing length	[29]
03	By use of template	undulating film-like structure to inverse opal like structure	[20]
04	By increasing electrodeposition time	smooth to typical sea-island like morphology	[30]
05	By using template and annealing treatment	non porous nano-particles to nano-rods	[31]

D) Supercapacitive study:

Here we have summarized the supercapacitive study of electrodeposited vanadium pentoxide thin films. Supercapacitive study will be analyzed with the help of cyclic voltammetry, Galvanostatic charge-discharge (GCD) study and electrochemical impedance study. Here we are comparing the values of specific capacitance either it may be calculated from the cyclic voltammetry study or it may be calculated from GCD study. Table 3 shows the comparative study of values of specific capacitance. From this comparative study, other researcher can get the information about electrolyte, potential windows, value of specific capacitance etc.

Table 3: Comparative study of specific capacitance of electrodeposited vanadium pentoxide thin films

Sr. No.	Technique from which specific capacitance calculated	Parameters	Electrolyte	Specific capacitance	Ref.
01	Cyclic Voltammetry study	Scan rate: 2 $mV.s^{-1}$ with respect to a Ag/AgCl reference electrode Potential window: from – 0.2 V to 0.8 V	2 M KCl electrolyte	214 $F.g^{-1}$	[24]
02	Cyclic Voltammetry study	Scan rate: 10 $mV.s^{-1}$ vs SCE Potential window: from – 0.2 V to 0.6 V	0.5 M K_2SO_4 electrolyte	279 $F.g^{-1}$	[32]
03	GCD method	Current density: 1 $A.g^{-1}$	0.5 M $LiClO_4$ in PC	657 $F.g^{-1}$	[28]
04	Cyclic Voltammetry study	Scan rate: 5 $mV.s^{-1}$ vs SCE Potential window: from –1.3V to –0.1 V	1 M KCl	608 $F.g^{-1}$	[33]
05	Cyclic Voltammetry study	Scan rate: 5 $mV.s^{-1}$ vs Ag/AgCl Potential window: from – 0.2 V to 0.8 V	3 M KCl	350 $F.g^{-1}$	[34]

III.CONCLUSION

The VO thin films will be electrodeposited by three different modes like potentiostatic mode, galvanostatic mode and potentiodynamic mode. The working electrode would be any conducting substrate used in electrodeposition of VO thin films. The role of precursor and its concentration is important in electrodeposition because the oxidation potentials may be differ for precursors and its concentrations. The structural investigations showed that as deposited films are amorphous in nature, so for crystalline nature it is necessary to anneal the samples at 500 °C. So annealing of sample are prime requirement for good crystalline nature of samples. From morphological study, it is evident that the as deposited films are smooth in nature i.e. they are featureless in nature, for further use it is necessary to modify the samples by the use of in-situ and ex-situ treatments such as Electrodeposition time, Electrodeposition mode, use of template, annealing of samples etc then samples changes to nano-plates or

nanostructures etc. In supercapacitive study it is evident that the specific capacitance can be calculated either from cyclic voltammetry or galvanostatic charge-discharge study. It is evident that different electrolytes for VO thin films have different potentials windows (for CV study) and different loads of current density (for GCD study). So, this mini review will help to new researcher to get proper idea of Electrodeposition of VO thin films and its structural, morphological study along with supercapacitive study.

IV. REFERENCES

[1]. A. C. Sonavane, A. I. Inamdar P. S. Shinde, H. P. Deshmukh R. S. Patil P. S. Patil, Efficient electrochromic nickel oxide thin films by Electrodeposition, Journal of Alloys and Compounds, 489(2010) 667

[2]. Y. Tang, Z. Chen, Z. Jia, L. Zhang, J. Li, Electrodeposition and characterization of nanocrystalline cuprous oxide thin films on TiO2 films, Materials Letters, 59(2005)434

[3]. G. Machado, D. N. Guerra, D. Leinen, J. R. Ramos-Barrado, R. E. Marotti, E. A. Dalchiele, Indium doped zinc oxide thin films obtained by Electrodeposition, Thin Solid Films, 490(2005) 124

[4]. T. Yoshida, D. Komatsu, N. Shimokawa, H. Minoura, Mechanism of cathodic electrodeposition of zinc oxide thin films from aqueous zinc nitrate baths, Thin Solid Films, 451–452(2004)166

[5]. R. S. Patil, M. D. Uplane, P. S. Patil, Structural and optical properties of electrodeposited molybdenum oxide thin films, Applied Surface Science, 252(2006)8050

[6]. M. Nakayama, A. Tanaka, Y. Sato, T. Tonosaki, K. Ogura, Electrodeposition of manganese and molybdenum mixed oxide thin films and their charge storage properties, Langmuir 21(2005)5907

[7]. T. D. Golden, A. Q. Wang, Anodic Electrodeposition of Cerium Oxide Thin Films: II. Mechanism Studies, Journal of The Electrochemical Society 150(2003)C621

[8]. V. D. Patake, C. D. Lokhande, O. S. Joo, Electrodeposited ruthenium oxide thin films for supercapacitor: Effect of surface treatments, Applied Surface Science, 255(2009)4192

[9]. D. Rehnlund, M. Valvo, K. Edström, L. Nyholm, Electrodeposition of Vanadium Oxide/Manganese Oxide Hybrid Thin Films on Nanostructured Aluminum Substrates, Journal of The Electrochemical Society, 161 (2003)D515

[10]. L. Li, S. Peng, H.Y. Chen, X. Han, F. Cheng, M. Srinivasan, S. Adama, S. Ramakrishna, J. Chen, Polypyrrole-coated hierarchical porous composites nanoarchitectures for advanced solid-state flexible hybrid devices, Nano Energy, 19(2016)307

[11]. N. Ozer, C.M. Lampert, Electrochromic performance of sol-gel deposited WO3–V2O5 films, Thin Solid Films, 349(1999)205

[12]. J.K. Lee, G.P. Kim, I.K. Song, S.H. Baeck, Electrodeposition of mesoporous V2O5 with enhanced lithium-ion intercalation property, Electrochem. Commun. 11(2009)1571

[13]. S. Papaefthimiou, G. Leftheriotis, P. Yianoulis, Study of electrochromic cells incorporating WO3, MoO3, WO3-MoO3 and V2O5 coatings, Thin Solid Films, 343(1999)183

[14]. C.E. Patil, N.L. Tarwal, P.S. Shinde, H.P. Deshmukh, P.S. Patil, Synthesis of electrochromic vanadium oxide by pulsed spray pyrolysis technique and its properties, J. Phys. D, 42(2009) 025404

[15]. S. Capone, R. Rella, P. Siciliano, L. Vasanelli, A comparison between V2O5 and WO3 thin films as sensitive elements for NO detection, Thin Solid Films, 350(1999)264

[16]. J. Zheng, Y. Zhang, X. Jing, Q. Wang, T. Hu, N. Xing, C. Meng, Improvement of the specific capacitance of V2O5 nanobelts as

supercapacitor electrode by tungsten doping, Materials Chemistry and Physics, 186(2017)5

[17]. E. Andrukaitis, Lithium intercalation in electrodeposited vanadium oxide bronzes, Journal of Power Sources, 119–121(2003)205

[18]. R. Apostolova, B. Markovsky, D. Aurbach, E. Shembel, Effect of Superhalogen Anions on the Electrochemical Behavior of V2O5 Electrodes in Redox Reactions with Lithium in EC-DMC/Li-Salt Solutions, ECS Transactions, 95 (1) 183-200 (2019)

[19]. E. A. A. Arbab, G. T. Mola, V2O5 thin film deposition for application in organic solar cells, Appl. Phys. A 122 (2016)405

[20]. E. Armstrong, D. McNulty, H. Geaney, C. O'Dwyer, Electrodeposited Structurally Stable V2O5 Inverse Opal Networks as High Performance Thin Film Lithium Batteries, ACS Applied Materials & Interfaces, 7(2015)27006

[21]. M. H. Bai, L. J. Bian, Y. Song, X. X. Liu, Electrochemical codeposition of Vanadium Oxide and Polypyrrole for High Performance Supercapacitor with High Working Voltage, ACS Applied Materials & Interfaces, 6(2014)12656

[22]. J. A. Bennett, J. E. Pander III, M. A. Neiswonger, Investigating the viability of electrodeposited vanadium pentoxide as a suitable electrode material for in vivo amperometric hydrogen sulfide detection, Journal of Electroanalytical Chemistry, 654 (2011) 1

[23]. M. Chen, X. Xia, J. Yuan, J. Yin, Q. Chen, Free-standing three-dimensional continuous multilayer V2O5 hollow sphere arrays as high-performance cathode for lithium batteries, Journal of Power Sources, 288 (2015) 145

[24]. A. Ghosh, E. J. Ra, M. Jin, H. K. Jeong, T. H. Kim, C. Biswas, Y. H. Lee, High Pseudocapacitance from Ultrathin V2O5 Films Electrodeposited on Self-Standing Carbon-Nanofi ber Paper, Adv. Funct. Mater. 21(2011) 2541

[25]. D. V. Raj, V. Nandhinidevi, D. Mangalaraj, C. Viswanathan, Electrodeposition of V2O5 nanorods on current collector substrate, AIP Conf. Proc., 1447(2012)435

[26]. L. Tsui, H. Hildebrand, J. Lu, P. Schmuki, G. Zangari, Metal-insulator transition in nanocomposite VOx films formed by anodic electrodeposition, Applied Physics Letters, 103(2013)202102

[27]. D. Yu, Y. Qiao, X. Zhou, J. Wang, C. Li, C. Chen, Q. Huo, Mica-like vanadium pentoxide-nanostructured thin film as high-performance cathode for lithium-ion batteries, Journal of Power Sources, 266(2014)1

[28]. A. Aamir, A. Ahmad, Y. Khan, Z. U. Rehman, N. U. Ain, S. K. Shah, M. Mehmood, B. Zaman, Electrodeposited thick coatings of V2O5 on Ni foam as binder free electrodes for supercapacitors, Bull Mater Sci, 43(2020)273

[29]. T. K. Le, M. Kang, S. W. Kim, Room-temperature photoluminescence behavior of α-V2O5 and mixed α-β phase V2O5 films grown by electrodeposition, Materials Science in Semiconductor Processing, 94 (2019) 15–21

[30]. Y. R. Lu, T. Z. Wu, C. L. Chen, D. H. Wei, J. L. Chen, W. C. Chou, C. L. Dong, Mechanism of electrochemical deposition and coloration of electrochromic V2O5 nano thin films: an in situ x-ray spectroscopy study, Nanoscale Research Letters, 10 (2015)387

[31]. Y. Lu, X. Zhou, Synthesis and characterization of nanorod-structured vanadium oxides, Thin Solid Films, 660 (2018) 180

[32]. M. A. Sutar, M. S. Pawar, M. K. Rendale, S. K. Kandalkar, Effect of annealing on super-capacitive performance of electrodeposited vanadium-nickel oxide thin film electrode, Imperial Journal of Interdisciplinary Research (IJIR), 2(5)(2016)595

[33]. R. S. Ingole, B. J. Lokhande, Electrochemically synthesized mesoporous architecture of vanadium oxide on flexible stainless steel for high performance supercapacitor, J Mater Sci: Mater Electron, 28(2017)10951

[34]. J. D. Xie, H. Y. Li, T. Y. Wu, J. K. Chang, Y. A. Gandomi, Electrochemical energy storage of nanocrystalline vanadium oxide thin films prepared from various plating solutions for supercapacitors, Electrochimica Acta, 273 (2018) 257

International e-Conference on Recent Trends in Nano-Materials and Its Applications-2021
In Association with International Journal of Scientific Research in Science and Technology
Volume 9 | Issue 2 | Print ISSN: 2395-6011 | Online ISSN: 2395-602X (www.ijsrst.com)

Electrochemical Polymerization of Polypyrrole Thin Film by Potentiostatic Mode

J. V. Thombare[1]*, R. S. Gaikwad[1], P. M. Kharade[2], S. D. Patil[3], V. S. Shinde[4], S. S. Dhasade[1]

[1]Vidnyan Mahavidyalaya, Sangola, Tal-Sangola, Dist-Solapur, Maharashtra-413307, India
[2]Shankarrao Mohite Mahavidyalaya, Akluj, Dist-Solapur, Maharashtra, India
[3]Pratapsinh Mohite Mahavidyalaya, Karmala, Dist-Solapur, Maharashtra, India
[4]Baburao Patil College of Arts and Science, Anagar, Tal-Mohol, Dist-Solapur, Maharashtra, India

ABSTRACT

Polypyrrole thin films are prepared by electrodeposition. Here we have studied the film formation mechanism of polypyrrole thin films. The electrochemical oxidation of pyrrole makes a radical cation and di-cation. Initially, the concentration of radical cations is much higher than that of the neutral monomers which are near the electrodes, where, reactions are occurring and hence because of coupling di-cation forms. After losing two protons from di-cation again a neutral dimer is formed, which is then oxidized to radical cations, and so polymerization goes on. Polymerization and chain termination takes place in the gestation period.

Keywords : Electrodeposition, Potentiostatic Mode, Thin Films, Polypyrrole, etc.

I. INTRODUCTION

Electrochemical polymerization is the most widely used method in polypyrrole studies, offers many advantages [1-10]: it enables to produce an easily prepared polypyrrole with high conductivity, and in situ coating of polypyrrole on rather complex geometries. Electrochemical polymerization does not necessitate annealing at high temperature; therefore, it can be employed in flexible the devices such as dye sensitized solar cells (DSCs) [1], supercapacitors, etc. Polypyrrole films have been easily prepared either chemically or electrochemically. Polypyrrole is amorphous and conducting type conjugated polymer. Basically, polypyrrole has been made conductive by oxidation of the monomer i.e. pyrrole and conjugation have made with the anion. Due to conjugation with anion, the band gap energy of polypyrrole greatly reduced. Such conjugation with anion is called doping of polypyrrole by anion [11-12]. Polypyrrole has lots of distinct features related to electrical conductivity, electroactivity and high environmental stability, so it attracts widespread research interests [13].

Conducting polypyrrole shall be prepared electrochemically, by applying a potential across a solution containing the pyrrole to be polymerized and an electrolyte (supporting electrolyte), or chemically; using oxidants or cross-coupling catalysts. One of the advantages of electrochemical polymerization is that, the yielded polypyrrole electrodeposited in the form of film on the anode. However, anodic

electropolymerization has a serious shortcoming; the electro-generated polypyrrole presents structural irregularities due to polymer cross-linking [14]. Conducting polypyrrole is a promising electrode material for redox capacitors as, it is less expensive than other electrode materials, e.g., noble metal oxides [15].

This chapter deals with synthesis and characterization of polypyrrole films by potentiostatic mode of electrodeposition. The variation of current with voltage is studied with the help of linear sweep voltammetry and the deposition potential i.e. oxidation potential of polypyrrole is determined and polypyrrole films were deposited accordingly.

II. EXPERIMENTAL PROCESSES (POLYPYRROLE FILM FORMATION):

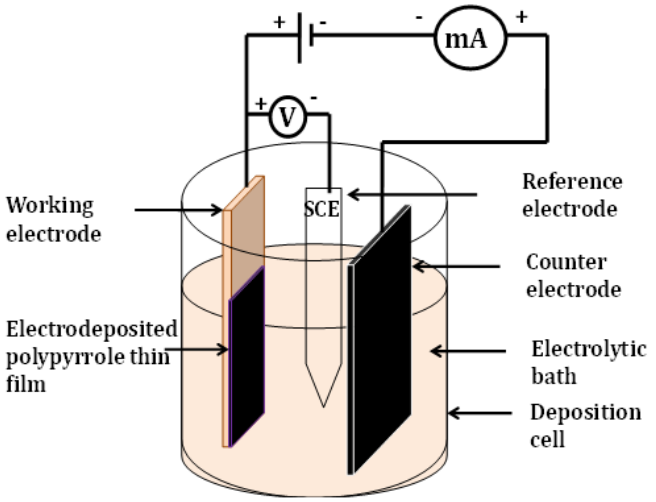

Fig. 1: Electrodeposition set up for synthesis of polypyrrole films

The room temperature deposition keeps away from the oxidation and corrosion of metallic substrates. Preparative parameters such as deposition potential, deposition time and concentration of the precursor optimized. In the typical synthesis, (0.1 M) pyrrole and (0.5 M) sulphuric acid are used as the monomer and electrolyte, respectively. Polypyrrole films were prepared on stainless steel substrates, at deposition potential of + 0.7 V vs SCE. The polypyrrole film was deposited on anode (stainless steel) and a pure graphite plate having nearly equal to area 4 cm^2 (Size:1 cm X 4 cm) of working electrode was used as a cathode, a saturated calomel electrode (SCE) was used as the reference electrode. A black colored polypyrrole film was obtained on the substrate as shown in Fig.1.

2.1. Substrate cleaning

Substrate cleaning is the breaking of the bonds between substrate and contaminants without detrimental the substrates. In thin film deposition process, substrate cleaning is an essential factor to get reproducible films as it affects the adherence, uniformity, smoothness and porosity of the films. The substrate cleaning process depends upon the nature of the substrate; degree of cleanliness required and nature of contaminates to be disinterested. The common contaminates are grease, oil particles, air borne dust, lint, adsorbed water etc. The stainless steel has been used as substrates. The following process has been assumed for cleaning the substrates.

1. The substrates were washed with detergent solution 'Molyclean' and then with water.
2. These substrates were boiled in chromic acid for about five minutes and then rinsed with distilled water.
3. These substrates were kept in NaOH solution to remove the acidic contaminations, washed with distilled water and cleaned ultrasonically.
4. Finally, the substrates were air dried.

III. RESULTS AND DISCUSSION

3.1 Mechanism of the Polymerization

In an electrochemical polymerization of pyrrole, the monomer pyrrole was dissolved in a solvent containing the anionic doping species such as H_2SO_4 (in present case), is oxidized at the surface of an electrode by application of an anodic potential (oxidation). The choice of the solvent and electrolyte is of particular importance in electrochemistry. Since, both solvent and electrolyte should be stable at the

oxidation potential of the monomer and provide an ionically conductive medium. Since pyrrole has a relatively low oxidation potential [16], electropolymerization shall be carried out in aqueous electrolytes.

As a result of the initial oxidation, the radical cation of the pyrrole is formed and reacts with other monomers present in solution to form oligomeric products and then the polymer. The extended conjugation in the polymer results in a lowering of the oxidation potential compared to the monomer. Therefore, the synthesis and doping of the polymer are generally done simultaneously. The anion is incorporated into the polymer to ensure the electrical neutrality of the film and at the end of the reaction, a polymeric film of controllable thickness is formed at the anode. The anode can be made of a variety of materials including platinum, gold, glassy carbon, stainless steel and tin doped indium oxide (ITO) coated glass. In the present work, we used the 304 stainless steel substrate as working electrode for deposition of polypyrrole thin film.

The electropolymerization is achieved by potentiostatic deposition mode corresponding to a constant potential applied at the surface of the electrode. The polymerization mechanism between chemical and electrochemical polymerization is different, only initial step is same i.e. generation of radical cations, which is shown in Fig.2. In this case, the concentration of radical cations is much higher than that of the neutral monomers which are near the electrodes, where, reactions are occurring and radical-radical coupling forms di-cation. Then di-cation loses two protons, generating a neutral dimer, which is then oxidized to radical cations, and so polymerization goes on. These radical cations, dimmers and trimmers are formed in the small "gestation period", before the polymerization [17].

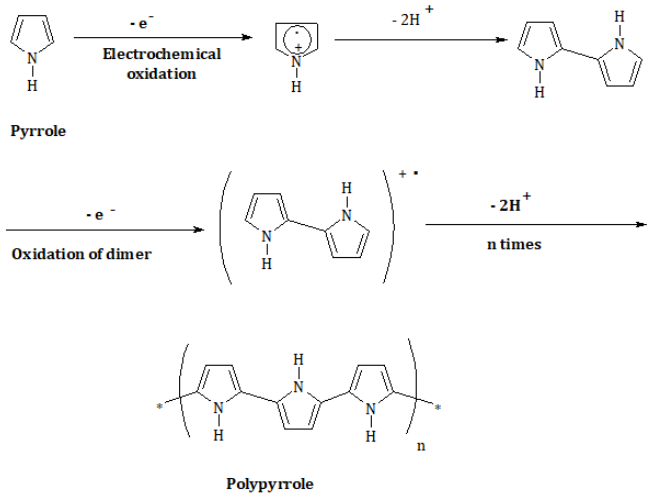

Fig.2: Polymerization mechanism of electrochemically synthesized polypyrrole films

IV. CONCLUSION

As per study, the electrodeposition of polypyrrole thin films at room temperature is easy process also there is no need of any sophisticated instruments. Also, with the help of electrodeposition we can control the film properties such as thickness, electrical conductivity etc. From electrochemical polymerization study we understand the formation of pyrrole ions, dimmers and so on i.e. formation of polymer chain.

V. REFERENCES

[1]. T. Makris, V. Dracopoulos, T. Stergiopoulos, P. Lianos, Electrochimica Acta, 56 (2011) 2004

[2]. R. Ramola, S. Chandra, J. Rana, R. Sonkawade, P. Kulriya, F. Singh, D. Avasthi, S. Annapoorni, Journal of Physics D: Applied Physics, 41 (2008) 115411

[3]. A. Ramanaviciene, W. Schuhmann, A. Ramanavicius, Colloids and Surfaces B: Biointerfaces 48 (2006) 159

[4]. Y. Cho, R. Borgens, Langmuir, 27 (2011) 6316

[5]. J. Lee, F. Serna, C. Schmidt, Langmuir 22 (2006) 9816

[6]. H. Bai, Q. Chen, C. Li, C. Lu, G. Shi, Polymer, 48 (2007) 4015

[7]. V. Misoska, J. Ding, J. Davey, W. Price, S. Ralph, G. Wallace, Polymer, 42 (2001) 8571 [8] A. Hussain, D. Saikia, F. Singh, D. Avasthi, A. Kumar, Nuclear Instruments and Methods in Physics Research B, 240 (2005) 834

[8]. I. Vermeir, N. Kim, P. Laibinis, Applied Physics Letters, 74 (1999) 3860

[9]. P. Somani, S. Radhakrishnan, Chemical Physics Letters, 292 (1998) 218

[10]. R. J. Waltman, J. Bargon, Candian Journal of Chemistry, 64 (1986) 76

[11]. N. K. Guimard, N. Gomez, C. E. Schmidt, Progress in Polymer Science, 32 (2007) 876 [13] Y. Lan, E. Wang, Y. Song, Y. Song, Z. Kang, L. Xu, Z. Li, Polymer, 47 (2006) 1480 [14] C. Aleman, J. Casanovas, J. Torras, O. Bertran, E. Armelin, R. Oliver, F. Estrany, Polymer, 49 (2008) 1066

[12]. A. Hussain, A. Kumar, Journal of Power Sources, 161 (2006) 1486

[13]. S. Sadki, P. Schottland, N. Brodiec, G. Sabouraud, Chemical Society Reviews, 29 (2000) 283

[14]. P. Chandrasekhar, Conducting polymers, Fundamentals and applications: a practical approach, Technology and Enginnering, Springer, 1999.

International e-Conference on Recent Trends in Nano-Materials and Its Applications-2021
In Association with International Journal of Scientific Research in Science and Technology
Volume 9 | Issue 2 | Print ISSN: 2395-6011 | Online ISSN: 2395-602X (www.ijsrst.com)

Electrochemical Synthesis of Manganese Oxide Thin Film for Super Capacitor

P. M. Kharade[1*], J. V. Thombare[2], S. D. Patil[3], S.S. Dhasade[2], P.B.Abhange[4], R. S. Gaikwad[5], C.S. Pawar[1], S. S. Deokar[1], D.J. Salunkhe[6]

[1]Department of Physics, Shankarrao Mohite Patil Mahavidyalaya, Akluj, Dist-Solapur, Maharashtra, India
[2]Department of Physics, Vidnyan Mahavidyalaya, Sangola, Dist-Solapur, Maharashtra, India
[3]Department of Physics, Pratapsingh Mohite Mahavidyalaya, Karmala, Dist-Solapur Maharashtra, India
[4]Department of Physics, G.M. Vedak College of Science, Tala, Raigad, Maharashtra, India
[5]Department of Chemistry, Vidnyan Mahavidyalaya, Sangola, Dist-Solapur, Maharashtra, India
[6]Nanocomposite Research Laboratory, K.B.P. Mahavidyalaya, Pandharpur, Dist-Solapur, Maharashtra, India

ABSTRACT

In the present investigation, we report synthesis of manganese dioxide (MnO2) thin film on low cost conducting substrate by electrodeposition method for supercapacitor application. The structural and surface wettability study of MnO2thin film was carried out with the help of X-ray diffraction (XRD) and contact angle meter. The supercapacitive properties of MnO2 thin film were carried out by using cyclic voltammetry (CV), charging-discharging (CD) study. The electrodeposited MnO2thin film shows specific capacitance of 430 F/g-at 10 mV/S scan rate. The specific energy and power of MnO2thin film were 7.40 kW/kg and 3.20 Wh/kg respectively. Hence, electrodeposited MnO2thin film is best electrode candidate for energy storage.

Keywords: supercapacitor, electrodeposition, MnO2, XRD, Cyclic voltammetry.

I. INTRODUCTION

In the recent years there is an urgent need of clean, renewable and sustainable energy storage devices. One such devices, supercapacitor or electrochemical capacitor plays key role in development of energy storage devices. It has higher energy density as compared to conventional capacitor and greater power densities than batteries.Supercapacitor have fascinated more attention due to outstanding electrochemical characteristics viz high power density, long capacitance retention ratio, good reversibility, environmental friendless, etc. The supercapacitor or electrochemical capacitor is broadly classified into two types depends on their charge storage mechanism such as electrochemical double capacitor and pseudocapacitor. In electrochemical double layer capacitor (EDLCs) charge storage takes place non faradically. Carbon based electrode material used in EDLCs. In pseudocapacitor charge storage takes place faradically. The conducting polymers and transition metal oxides are used as electrode material in pseudocapacitor. Manganese oxide is mostly studied as electrode material in transition metal oxide

family due to their excellent electrochemical properties such as, non-toxic, cheaper in cost, easy synthesis and variable oxidation states.It is used in catalysis, sensors, supercapacitor, rechargeable batteries and water waste treatment [1-5]. Manganese oxide electrode have been synthesized by various physical and chemical methods. Different synthesis methods gives different microstructures of manganese oxide. In supercapacitor nanocrystalline and hydrophilic electrode is mostly used for supercapacitor application. It provide higher surface area, more interaction of ions from electrode to electrolyte interface and shorten the diffusion path length which strongly improve the supercapacitive performance.

In the present work, efforts have been taken to synthesize manganese oxide electrode by potentiostatic electrodeposition method. There supercapacitive performance was tested by using cyclic voltammetry, charging-discharging studies.

II. EXPERIMENTAL

2.1. Synthesis of Manganese Dioxide (MnO_2) Thin Films:

Manganese Dioxide (MnO_2) thin filmwas carried out using a two-electrode system. Graphite sheet was served as counter electrode. Stainless steel substrate was used as working electrode. For synthesis of Manganese Dioxide (MnO_2) thin film, the aqueous bath contain 0.2M $MnCl_2$ aqueous solution. The Prior to deposition the stainless steel (SS) was used as substrate and it is well polished with zero grade polish paper rough to finish and rinsed with double distilled water and acetone. The MnO_2 thin film was deposited by using potentiostatic electrodeposition method by keeping potential of 1.8 V for 15 minutes, manganese hydroxide was formed. Further oxidation of Mn, the film was annealed at 300˚C for one hour. The colour of Mn changes from yellowish to black brown. Then oxidized film was used for further characterization.

2.2. Characterization techniques:

The as synthesized MnO_2 thin film was characterized by using different characterization techniques. The crystal structure and surface wettability study of MnO_2 thin film was carried out with help of by X-ray diffraction (XRD) techniquesusing Bruker axes D8 Advance Model with copper radiation (Kα of λ = 1.54 A˚) in the 2θ range between 20˚ to 80˚ and Rame-Hart contact angle meter respectively. The electrochemical performance of MnO_2 thin film was studied by using cyclic voltammetry and charging-discharging study. An electrochemical cell consists of three electrode systems, MnO_2thin film as a working electrode, graphite as a counter electrode and saturated calomel electrode (SCE) as a reference electrode. All electrochemical measurement was carried out using aqueous 0.5 M Na_2SO_4electrolyte solution.

III. RESULTS AND DISCUSSIONS

3.1. Structural study:

X-ray diffraction (XRD) is an important tool to analyze the crystal structural information of synthesized thin film. Fig (1) shows the XRD spectra of potentiostatically deposited MnO_2 thin film within2θ range between 20˚ to 80˚. The XRD pattern of MnO_2 thin film electrode shows tetragonal crystal symmetry. The lattice parameter observed in these case are a= b=94.815 AU and c=2.847 AU. The peaks observed in the XRD spectrum of MnO_2 thin film electrode were well matched with JCPDS data (Card No 72.1982). The additional peaks indexed (SS) in the XRD spectra is due to the stainless steel substrate only. Thus, XRD study confirms the crystalline structure of deposited MnO_2 thin film.

3.2. Surface wettability study

The surface wettability study of film determines its ability to interact with ions when dipped into electrolyte, which is determined by measuring the contact angle with liquid electrolyte. If contact angle

is less than 90°, then the film surface is said to be hydrophilic, and for greater than 90°, it is said to be hydrophobic. For more interaction of electrolyte ions with electro active site on the surface of thin film, the contact angle must be as low as possible. Wettability of MnO_2 thin film is studied by measuring contact angle. Fig. (2) shows the images of contact angle with film surface. The observed value of contact angle for MnO_2 thin films is found to be 76°. Thus, wettability study shows hydrophilic nature of MnO_2 thin film. The hydrophilic nature of electrode is feasible for supercapacitor, which allows more interaction of electro active sites of MnO_2 thin film with electrolyte [6].

3.3. Supercapacitive Study:

3.3.1. Cyclic Voltammetry (CV) Study:

Cyclic voltammetry (CV) is a most important tool to give the qualitative information about redox process and specific capacitance associated with electrode. Fig. (4) shows typical cyclic voltammogram of MnO_2 thin film at 10 mV/s scan rate within potential range of +1.2 V to -1.2 V in 0.5 M Na_2SO_4 electrolyte solution. The nature of CV curve is nearly rectangular in shape indicating the ideal pseudocapacitor behaviour of deposited MnO_2 thin film. The specific capacitance of the MnO_2 thin film was calculated by using following formulae,

Specific capacitance (C_s) = C/W ------ (1)

Where, C – capacitance in farad and W – the mass of active electrode materials in gm. The active mass of MnO_2 thin film in gm. The calculated value of specific capacitance of MnO_2 thin film is 430 F/gat 10 mV/s scan rate. The greater value of specific capacitance in present case is nanocrystalline and hydrophilic nature of MnO_2 thin film.

3.3.2. Charging-discharging study:

The electrochemical supercapacitor parameter such as coulombic efficiency, specific energy and power of the electrode was carried out with the help of charging-discharging study. Fig. (4) shows the charging-discharging (CD) study of MnO_2 thin film at 10 mA current density. The nature of charge and discharge curve is triangular in shape. There is a small voltage drop at the starting of discharge curve is due to internal resistance present between the MnO_2 thin film and electrolyte. The electrochemical supercapacitor was calculated by the following formulae:

Coulombic Efficiency=T_d/T_cx100 (2)

Specific power =(V X I_d)/W (3)

Specific energy=(V X I_d X T_d)/W (4)

Where, T_d and Tc is discharging and charging time in sec, V is voltage window volt, I_d is discharging current in A and W is the weight of active material in gm.

The coulombic efficiency of MnO_2 thin film was found to be 94% whereas the specific power and specific energy were observed to be 7.40 kW/kg and 3.20 Wh/kg, respectively.

IV. CONCLUSION

In summary, we have synthesized MnO2 thin film by potentiostatic electrodeposition method for supercapacitor application. The XRD study show the tetragonal crystal structure. The wettability study shows MnO2 thin film is hydrophilic in nature. The MnO2 thin film gives maximum specific capacitance of 430 F/g. The MnO2 thin film shows values of specific energy and specific power isbe 7.40 kW/kg and 3.20 Wh/kg respectively. Thus potentiostatistically deposited MnO2 thin film is suitable material for energy storage devices.

V. REFERENCES

[1]. D. Yan, S. Cheng, R. F. Zhuo et al., “Nanoparticles and 3D sponge-like porous networks of manganese oxides and their microwave absorption properties,” Nanotechnology, 20(2009) 105706.

[2]. Y. W. Tan, L. R. Meng, Q. Peng, and Y. D. Li, "One-dimensional single-crystalline Mn3O4 nanostructures with tunable length and magnetic properties of Mn3O4 nanowires," Chemical Communications, 47 (2011)1172.

[3]. X. Zhang, Z. Xing, Y. Yu et al., "Synthesis of Mn3O4 nanowires and their transformation to LiMn2O4 polyhedrons, application of LiMn2O4 as a cathode in a lithium-ion battery," CrystEngComm, 14(2012) 1485.

[4]. R. Ma, Y. Bando, L. Zhang, and T. Sasaki, "Layered MnO2 nanobelts: hydrothermal synthesis and electrochemical measurement," Advanced Materials, 16(2004)918.

[5]. J. Cao, Q. H. Mao, L. Shi, and Y. T. Qian, "Fabrication of γ-MnO2/α-MnO2/ hollow core/shell structures and their application to water treatment," Journal of Materials Chemistry, 21(2011) 16210.

[6]. P.M. Kharade, S.B. Kulkarni, D.J. Salunkhe, Nanoflakes like hydrophilic Mn2O3 thin film as a supercapacitor electrode, Chinese J. Phy. 55 (2017)1684.

Figure:

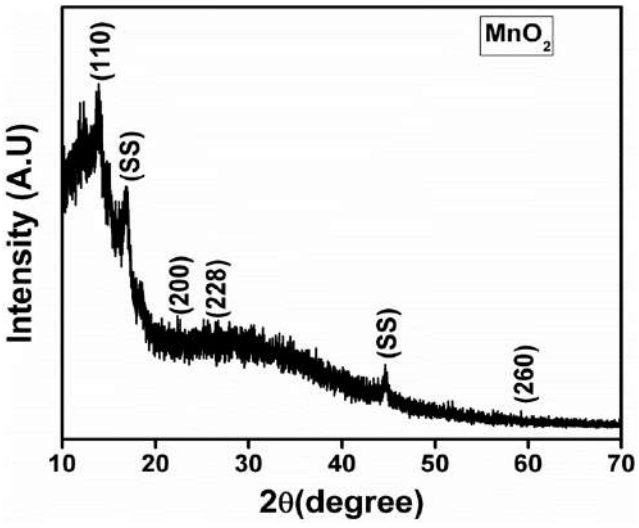

Fig. (1) XRD pattern MnO_2 thin film

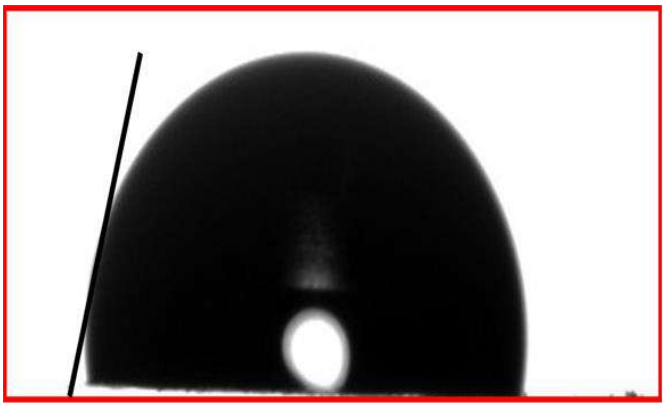

Fig. (2) Surface wettability of MnO_2 thin film

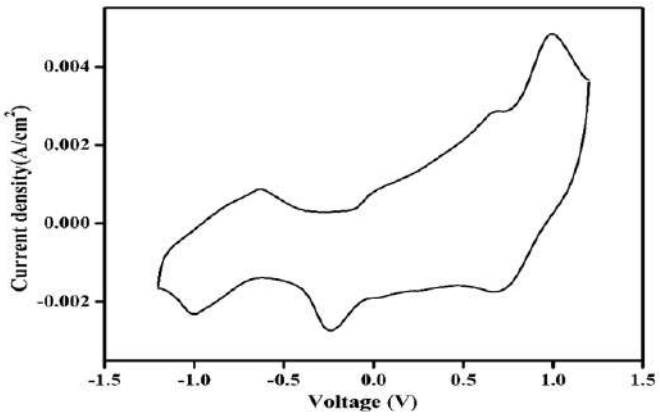

Fig. (3) CV of MnO_2 thin film

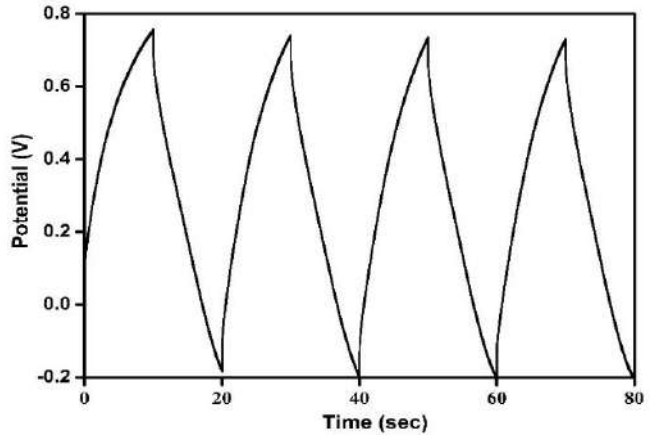

Fig. (4) Charging-discharging study of MnO_2 thin film

International e-Conference on Recent Trends in Nano-Materials and Its Applications-2021
In Association with International Journal of Scientific Research in Science and Technology
Volume 9 | Issue 2 | Print ISSN: 2395-6011 | Online ISSN: 2395-602X (www.ijsrst.com)

Structural and Wettability Study of Electrodeposited NiO Thin Film

P. M. Kharade[1*], A.R. Babar[1], J. V. Thombare[2], S. D. Patil[3], S.D.Chavan[4], D.J. Salunkhe[5]

[1]Department of Physics, Shankarrao Mohite Patil Mahavidyalaya, Akluj, Dist-Solapur, Maharashtra, India

[2]Department of Physics, Vidnyan Mahavidyalaya, Sangola, Dist-Solapur, Maharashtra, India

[3]Department of Physics, Pratapsingh Mohite Mahavidyalaya, Karmala, Dist-Solapur, Maharashtra, India

[4]Department of Physics, D.B.F. Dayanand College of Arts & Science, Solapur, Dist-Solapur, Maharashtra, India

[5]Nanocomposite Research Laboratory, K.B.P. Mahavidyalaya, Pandharpur, Dist-Solapur, Maharashtra, India

ABSTRACT

In the present paper, nickel Oxide (NiO) thin film has been synthesized by galvanostatic electrodeposition method. The crystal structural and surface wettability study of NiO thin film was carried out using X-ray diffraction (XRD) study and contact angle meter techniques. The XRD study reveals the cubic crystal structure of NiO thin film. The surface wettability study shows NiO thin film is hydrophilic in nature.

I. INTRODUCTION

Nickel Oxide (NiO) is asemiconducting oxide material having wide band gap lies between the ranges of 3.6 eV to 4 eV [1-2]. Nickel oxide (NiO) thin film have received great interest due to good electronic, optical and magnetic properties with high chemical stability. Due to these features it is used in variety of potential applications such as, fuel cell [3], gas sensors[4], solar thermal absorbers[5], photodetectors [6], batteries [7] and catalyst [8].

The NiO thin film have been synthesized by different physical and chemical methods such as, chemical bath deposition method [9], sputtering method [10], sol-gel method [11], chemical vapor deposition method [12], pulsed laser deposition [13]. The electrodeposition method is one of the best suitable method for deposition of metal on electrode substrate. Because it is cheap, easily available, and give thin, uniform film on substrate.

In the present work, NiO thin film has been synthesized by potentiostatic electrodeposition method. The structural and surface wettability study of NiO thin film was carried out with the help of characterized by X-Ray diffraction (XRD) and surface wettability study.

II. EXPERIMENTAL DETAILS:

2.1 Substrate Cleaning

Substrate cleaning is a most important part in the deposition of thin films. If the substrate surface is contaminated, the resulting films can be non-uniform. Electrically conducting substrate is the necessary requirement of electrodeposition. These substrates were cleaned using following procedure:

1) The substrates were mirror polished using zero grade polish paper.
2) The substrates were washed with detergent and double distilled water,

3) Finally, the substrates were dried, degreased in AR grade acetone and were kept in dust free chamber.

2.1.2 Synthesis of Nickel Oxide (NiO) Thin Films:

Nickel Oxide (NiO) thin films preparation was performed using a two-electrode system. Graphite sheet was served as counter electrode. Stainless steel substrate was used as working electrode. For electrodeposition bath of Nickel oxide thin film was prepared by AR grade chemicals using double distilled water. For synthesis of Nickel Oxide (NiO) thin film electrode, we have used 0.2M Nickel nitrate aqueous solution. Nickel Oxide (NiO) thin film electrode was deposited potentiostatically on stainless steel (SS) substrates with constant potentials of 1.9 V for 20 minutes and then Nickel hydroxide was formed. For oxidation of nickel, the films were annealed at 400˚C for one hour. This oxidized film was used for further characterization.

III. RESULTS AND DISCUSSION

3.1 X-ray diffraction study:

X-ray diffraction is a powerful technique to identify the crystal structure of the electrode materials. Fig.1 shows the XRD pattern of the film on to the stainless steel substrate with 2θ range of 20 to 80°. The XRD pattern of the film revealed the formation of NiO with cubic crystal structure. The main peaks are indexed at (2θ) 37.37˚ (111), 43.6˚(200) and 62.94° (220) reflections which are in good agreement with the standard diffraction pattern of NiO cubic structure (JCPDS card no. 47-1049). In addition with this, peaks originated due to stainless steel substrate are indicated by 'SS'. Justin et al have reported similar kind of crystal structure for NiO material prepared by hydrothermal method using organic surfactants as templates [14].

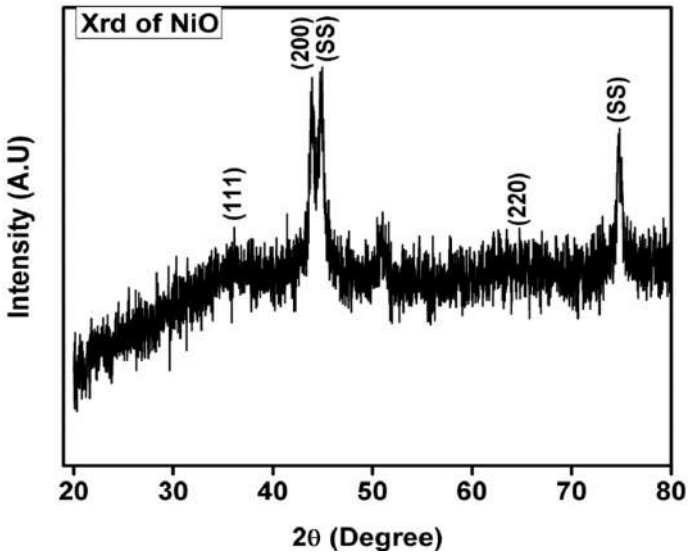

Fig.1 : X-ray diffraction study of NiO thin film.

3.2 Surface Wettability study:

Surface wettability study of the electrode was carried out with the help of water contact angle measurement with water as liquid drop.

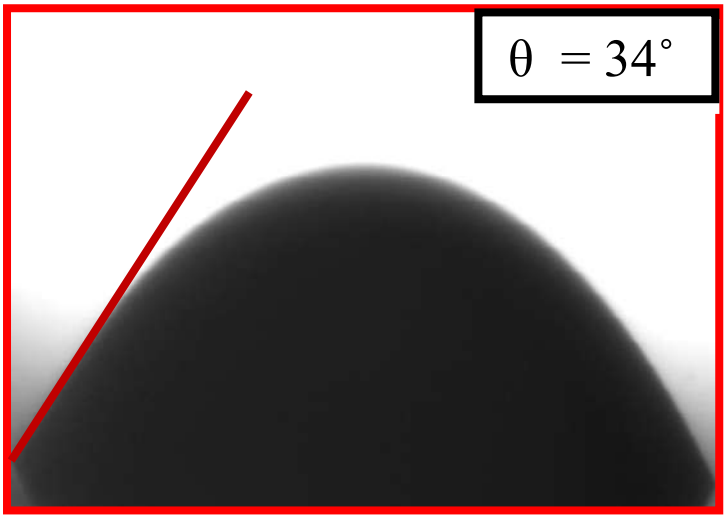

Fig.2 : contact angle of NiO thin film

The surface wettability study of film determines its ability to interact with ions when dipped into electrolyte, which is determined by measuring the contact angle with liquid electrolyte. Surface wettability of NiO thin film was studied by measuring contact angle. Fig.2 indicates the actual photograph of contact angle with film surface. The measured angle for NiO thin films is 34˚. In this study, it is observed that the NiO thin films are hydrophilic in nature and

contact angle for NiO decreases with increase in deposition cycles. The hydrophilic nature of film surface allows more interaction of electro active sites of NiO thin film.

IV. CONCLUSION

In the present report, we have synthesized nickel oxide (NiO) thin film on stainless steel substrates by using simple and economical potentiostatic electrodeposition method. The crystal structure and wettability study was carried out by using x-ray diffraction (XRD) and water contact angle measurements. The XRD study shows cubic crystal structure of electrodeposited NiO thin films. The surface wettability study shows NiO thin films are hydrophilic in nature.

V. REFERENCES

[1]. M. Guziewicz, et al., "Electrical and optical properties of NiO films deposited by magnetron sputtering," OpticaApplicata, vol. XLI, no. 2, pp. 431-440, 2011.

[2]. P. S. Patil and L. D. Kadam, "Preparation and characterization of spray pyrolyzed nickel oxide (NiO) thin films," Appl. Surf. Sci., vol. 199, pp. 211-221, 2002.

[3]. N.Shaigan, D.G.Ivey and W.Chen, "Metal-oxide scale interfacial imperfections and performance of stainless steels utilized as interconnects in solid oxide fuel Cells", J. Electrochem Soc., vol. 156, pp.B765-B770, 2009.

[4]. I. Hotovy, J. Huran, L. Spiess, R. Capkovic, S. Hascik, "Preparation and characterization of NiO thin films for gas sensor application, Vacuum 58 (2-3), (2000), pp. 300-307.

[5]. R. Cerc Korosec, P. Bukovec, B. Pihlar, A. SureaVuk, B. Orel and G. Drazie, "Preparation and structural investigation of electrochromic nanosizedNiOx films made via the sol-gel route" Solid State Ionics, vol.165, pp.191-200, 2003.

[6]. Leong-M. Choi, IM Seongil, "Ultrafiolet enhanced Siphotodetector using p-NiO films", Applied Surface Science 244(1-4), (2005), pp. 435-438.

[7]. C.M. Lambert and G. Nazri, P.C. Yu, "Spectroscopic and electrchemical studies of electrochromic hydrated nickel oxide

[8]. W. Azelee, W. Abu Bakar, M. Yusuf Othman, R. Ali , C. Yong, and S. Toemen, "The investigation of active sites on nickel oxide based catalysts towards the in-situ reactions of methanation and desulfurization," Modern Applied Science, vol. 3, no. 2, pp. 35- 43 ,2009.

[9]. E. Fujii, A. Tomozawa, H. Torii, and R. Takayama, "Preferred orientations of NiO films prepared by plasma-enhanced metalorganic chemical vapor deposition," Jpn. J. Appl. Phys., vol. 35, pp. L328-L330, 1996.

[10]. I. Hotovq, D. Buc, S. Hascik, and O. Nennewitz, "Characterization of NiO thin films preppared by reactive sputtering," Vaccum, vol. 50, pp. 41-44, 1998.

[11]. L. Cattin, B. A. Reguig, A. Khelil, M. Morsli, K. Benchouk, and J. C. Bernede, "Properties of NiO thin films deposited by chemical spray pyrolysis using different precursor solutions," Appl. Surf. Sci., vol. 254, no. 18, pp. 5814-5821, 2008.

[12]. X. H. Xia, J. P. Tu, J. Zhang, X. L. Wang, W. K. Zhang, and H. Huang, "Electrochromic properties of porous NiO thin films prepared by a chemical bath deposition," Sol. Energy Mater. Sol. Cells, vol. 92, no. 6, pp. 628-633, 2008.

[13]. K. Ravichandran and P. Philominathan, "Fabrication of antimony doped tin oxide (ATO) films by an inexpensive, simplified spray technique using perfume atomizer," Mater. Lett., vol. 62, pp. 2980-2983, 2008.

[14]. P. Justin, S.K. Meher, G.R. Rao, J. Phys. Chem. C 114 (2010) 5203.

International e-Conference on Recent Trends in Nano-Materials and Its Applications-2021
In Association with International Journal of Scientific Research in Science and Technology
Volume 9 | Issue 2 | Print ISSN: 2395-6011 | Online ISSN: 2395-602X (www.ijsrst.com)

Sensitive and Selective Detection of H_2S Gas Using Al-Doped ZnO Thin-Film Sensors

Sagar M. Mane[1], Amol R. Nimbalkar[2*], Nilam. B. Patil[3], Swati Patil[4], Shankar S. Dhasade[5], Jagannath V. Thombare[5], Jae Cheol Shin[1]

[1]Department of Physics, Yeungnam University, Gyeongsan, Gyeongbuk 38541, Republic of Korea
[2]Department of Physics, DKASC College, Ichalkaranji, Maharashtra, India
[3]SIT, Polytechnic, Yadrav, Ichalkaranji, Maharashtra, India
[4]PratapsinghMohite Mahavidyalaya Karmala, Maharashtra, India
[5]Vidnyan Mahavidyalaya Sangola, Maharashtra, India

ABSTRACT

A simple sol–gel spin-coating technique is used for the synthesis of Al-doped ZnO (AZO) thin films. Then, the structural, optical,electrical,andH2S-sensing properties of the AZOthin filmsare investigated.A structural analysis confirmed the formation of a crystalline zinc oxide thin film. Moreover, the gas-sensing performance of the AZO thin films for H2S gas areinvestigatedat 250°C.Our results reveal that the ZnO thin film doped with 2 at% Al demonstratesgood sensitivity and selectivity and shows excellent reproducibility forH2S gas,therebyexhibitingasignificantenhancement in the gas-sensing properties of the Al-doped ZnO lattice.

Keywords : Selectivity, Sensors, Reproducibility, Thin Films;Sol–Gel

I. INTRODUCTION

Various natural and industrial processes around the world are known to produce colorless, extremely noxious, and flammable hydrogen sulfide (H_2S) gas with a carious-egg-like smell. H_2S is generallyproduced during natural gas manufacturing, at crude petroleum refineries, and from automobile exhausts [1]. Thelong-term lower-level exposure of H_2Shas been known tocause headaches, irritability, dizziness, fatigue, poor memory and concentration,and even death[1, 2].In light ofthese effects,it becomes important to develop and fabricate devices for the detection of H_2S gas, especially at lower concentrations.A number of factors have to be considered for gas sensor fabrication, out of which quick gas response, stability, and selectivity are the three major requirements foragas-sensing device.In the past few years, metal oxide films based onnanocrystalline ZnOhave been intensively studied as suitable materials for a gas-sensing deviceasthey havea higher surface-area-to-volume ratio, display electrical and thermal stability at higher temperatures,andare cheaper compared with other oxide materials [3].Furthermore, the creation ofan electronic defect in a ZnO film improves the influence of the partial pressure of oxygen on the conductivity ofthe film; this type of defect can be created usingan appropriate dopant[3].Various metallic dopantmaterials such as Al, Cu, Co, Sn, Fe, and In can bedoped in ZnO filmsto improveits gas-sensing performance [3, 4].The present work reports

the doping of Al in a ZnO lattice using the sol–gel fabrication of thin films and the H_2S gas-sensing properties of these films.

II. EXPERIMENTAL PROCEDURE

A synthesis procedure similar to that used in our previous study [5] was adopted forthe synthesis of Al-doped ZnO (AZO) thin films at1–4 at%. The structural analyses of the AZO thin films werestudiedusing a Bruker D2 phaser X-ray diffractometer.The optical absorption spectra of the synthesized AZO filmswere recorded using a UV–Vis-NIR V-770 (Jasco, Japan). Moreover, the DCconductivity of the synthesized AZO thin films was studiedusinga locally designed two-probe system in the temperature range 27–300°C.The gas-sensing properties of the AZO sensor films werestudied at 250°C.The AZOsensor film resistance was measured and recorded at 250°C in the presence of a test gas and ambient air by using a Keithley electrometer (6514 model, USA).The gas response (R_s) was determinedusing R_a /R_g forH_2S gas, where R_a = resistanceof the sensor in air,and R_g =resistance of the sensor in the presence of a test gas.

III. RESULTS AND DISCUSSION

A typical XRD pattern of 2 at% AZO filmat 2θ = 20to 90° is shown in Fig.1.The figure inset shows the diffraction peak (002). No effect is seen on other diffraction planes (except 002).The doping of Al confirmsthat the synthesized AZO films are crystalline with c-axis (002) plane orientation and possesshexagonal crystal structure as per JCPDS card No. 01-079-0205.In addition, it is observed that the peak intensity of (002) increases with the Al concentration up to 2 at% and reduces for higher at% doping (3 and 4 at%), whereas shifting of the peak toward a higher 2θ anglewithhigherAl concentration confirms the growth of the Al atom in the ZnO lattice. The crystallite size of the synthesized AZO films wasdetermined usingtheDebye–Scherrer formula [5]. The crystallite sizeswere found to be 32, 34, 35, 33, and 35 nm for 0, 1, 2, 3, and 4 at% AZO films, respectively.

The optical absorption of the sol–gel spin-coated AZO films was carried out with a wavelength range of 300–1000 nm. Figure 2 depictsthe plot of $(\alpha h\nu)^2$ versus photon energy ($h\nu$) for the AZO filmsaccording to Al-doping concentration (1–4 at%). From these plots, the opticalbandgap values were calculated using theTauc relation.The optical band gapvalueincreases from 3.21 to 3.26 eV as Al-doping concentration increases from 0 to4 at%, respectively.The increase inthe optical band gap with the Al doping concentration exhibits a goodcorrelation with the increase in the blueshift, which can be explained based onthe Burstein–Moss effect [6-7].

The DC conductivityof the AZO thin filmswas then measured in the temperature range 300–573K using a locally designed two-probe system.Figure 3shows thevariation in DCelectrical conductivity (σ)according to the temperature for theAZO thin films.The DCconductivity of the AZO filmsincreases exponentially with increase intemperatureand Al-doping concentration. The DCconductivity at room temperature is found to be between 4.85×10^{-7} S/cm and4.41×10^{-7} S/cm, which further increases and reaches a value between5.47×10^{-4} S/cm and 9.19×10^{-4} S/cm at 300°C for 0–4 at% AZO thin films, which confirms the semiconductor behavior of the AZO films [8].The plot of lnσ versus 1000/T for AZO thin filmsisshownin the inset of Fig.3.The activation energy was calculated from the slope of the lnσ versus 1000/T curve using the following equation:

$$\sigma = \sigma_o \exp(-E_a/KT) \quad (1)$$

where E_a= activation energy,σ_o = proportionality constant, K = Boltzmann constant,andT = temperature [9].The activation energy of the AZO thin filmsdecreases from 0.43 to 0.39 eV with increase inAl-doping concentration.These activation energy values illustrate that the excitation of thermally activated electrons from donor levels to the

conduction band is due to increase in temperature [10].

The gas response–recovery mechanism for the metal oxide sensor involves two key reactions: adsorption and desorption of O_2^-, O^-,and O^{2-} molecules by the sensing layer;these absorbed oxygen molecules trap the electrons from the conductance band and play a vital role in gas sensing.As a result,variations in the resistance of the sensor filmare observed [3].To determine the optimized Al-doping concentration in ZnO, the H_2S gas-sensing performance of AZO thin films is studiedas a function of gas concentration fora certain period oftime at 250°C.The gas response curves of the AZOfilms toward a fixed 50 ppmconcentration of H_2Sgas at 250°C are shown in Fig.4(a). Here, the 2 at% AZO sensor film demonstratesthehighestgas response compared with other films; therefore, 2 at% AZO is selected for theH_2Sgasresponse at variousconcentration levels.Figure4(b) shows the dynamic gasresponse of the 2 at% AZOfilm toward H_2S gas, which clearly shows that the sensor response improves (1.06 to 3.8) with increase in the gas concentration(5 to 50 ppm). The lower value of sensing response at lower levels of gas concentration can be attributed to H_2S gas molecules covering the sensing layer toa lesserextent, whereas at higher gas concentrations, H_2S gas molecules cover a greater part of the sensing layer area, thus resulting in maximum sensing response [4].

In general,the sensing consistency of a sensor mainly depends on the reproducibility demonstrated by the sensor material. To study the reproducibilityof the optimized Al-doped ZnO film for 2 at% doping, the gasresponse was assessed4 times at50 ppm H_2S gas concentrationat250°C,as shownin Fig.4(c).After four consecutive scans, the gas response of the 2 at% AZOfilm toward H_2Sgas remained nearly constant, which confirms the reproducibility of the as-synthesized Al-doped ZnO films for H_2Sgas sensing.The selectivity studies of the optimized 2 at% AZO film are performed at 250°C and 50 ppmfixed gas concentrationfor various gases, such as C_2H_5OH,CH_3OH, CH_3COCH_3, LPG, Cl_2, NH_3,andH_2S, as shown in Fig.4(c). From the figure, we can observe that the 2 at% AZO sensor film was comparatively sensitive,selective with higher selectivity coefficient,and showed higher gas response toward H_2S gascompared with other analyte gases.This higher sensitivity and selectivity of the Al-doped ZnO film at 2 at% makes it a promising material for the fabrication of gas-sensingdevices.

IV. CONCLUSION

AnH2Sgas sensor based on Al-doped ZnO thin films was fabricated using the less-expensive sol–gel spin-coating technique. The doping of a smaller amount of Alin a ZnO lattice results in changes in structural, optical, electrical,and H2Sgas-sensing properties. Gas-sensing studies ofa 2 at% Al-doped ZnO thin film at 250 °Crevealedthat it exhibited high gasresponse (3.8) with excellent reproducibility; it can also detect the low concentration of H2S gas with a realistic response (1.06). Therefore,weconclude that 2 at% Al-doped ZnO film is agood sensing material for H2S gas detection.

Acknowledgment

This study was supported by the National Research Foundation of Korea (NRF-2020R1A2C1015206).

V. REFERENCES

[1]. H.S. Woo, C.H. Kwak, I. D. Kim, and J.H. Lee, J. Mater. Chem. A.2, 6412 (2014).

[2]. S.S. Badadhe, I.S. Mulla, Sens. Act. B.143, 164 (2009).

[3]. S.S. Zahirullah, P. Immanuel, S. Pravinraj, P.F.H. Inbaraj, J.J. Prince, Mater. Lett.230, 1 (2018).

[4]. A.R. Nimbalkar, M.G. Patil, Mater. Sci.Semi. Pro. 71, 332 (2017).

[5]. N.B. Patil, A.R. Nimbalkar, M.G. Patil, Mater. Sci.Engg. B.227, 53 (2018).

[6]. F.K. Shan, Y.S. Yu, J.Euro. Ceram. Soc.24, 1869 (2004).
[7]. M.Vishwas, K.N. Rao, A.R. Phani, K.V.A. Gowda, R.P.S. Chakradhar, Solid State Comm.152, 324 (2012).
[8]. S.R. Aghdaee, V. Soleimanian, B. Tayebi, Superlatt. Micro.51, 149 (2012).
[9]. Y. Sahin, S.Öztürkb, N. Kılınc, A.Kösemen, M.Erkovan, Z.Z.Öztürk,App. Sur. Sci.303, 90 (2014).
[10]. Y.Caglar, M.Caglar, S.Ilican, Curr. App.Phy.12, 963(2012).

Figure captions

Fig.1XRD pattern of AZO thin films.
Fig.2$(\alpha hv)^2$versus hvcurves for AZO thin films.
Fig.3Plot of DC conductivity according to temperature; inset shows lnσversus 1000/T curves of AZO thin films.
Fig.4(a) Response of AZOsensor towards 50 ppm H_2S gas; (b)dynamic response, (c)reproducibility, (d) andselectivitystudy of 2 at% AZO film.

Figures

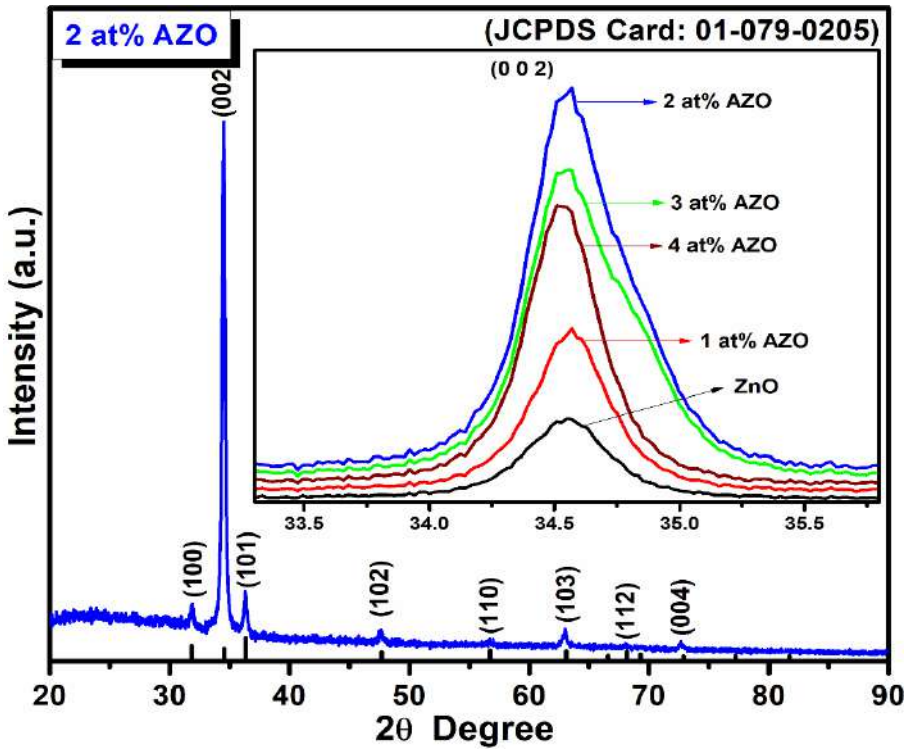

Figure: 1

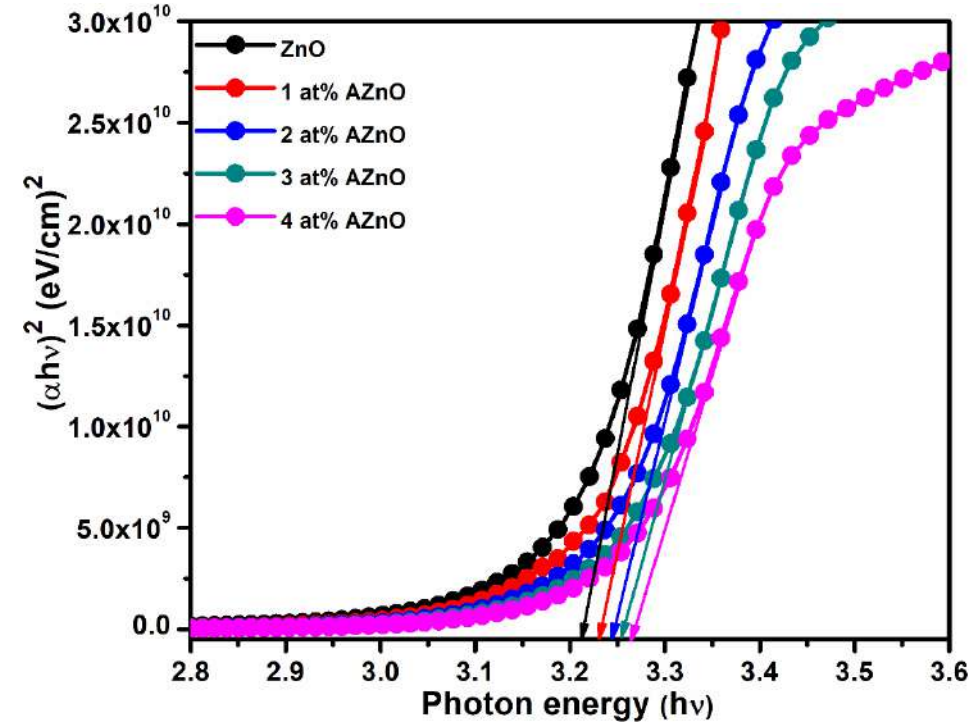

Figure: 2

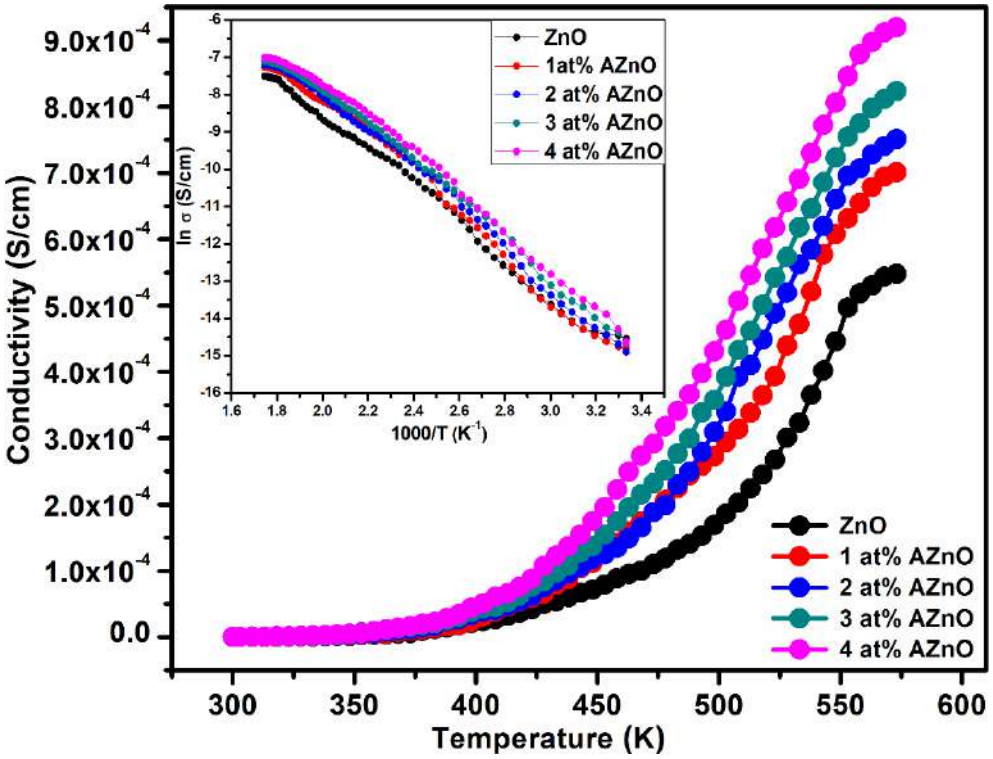

Figure: 3

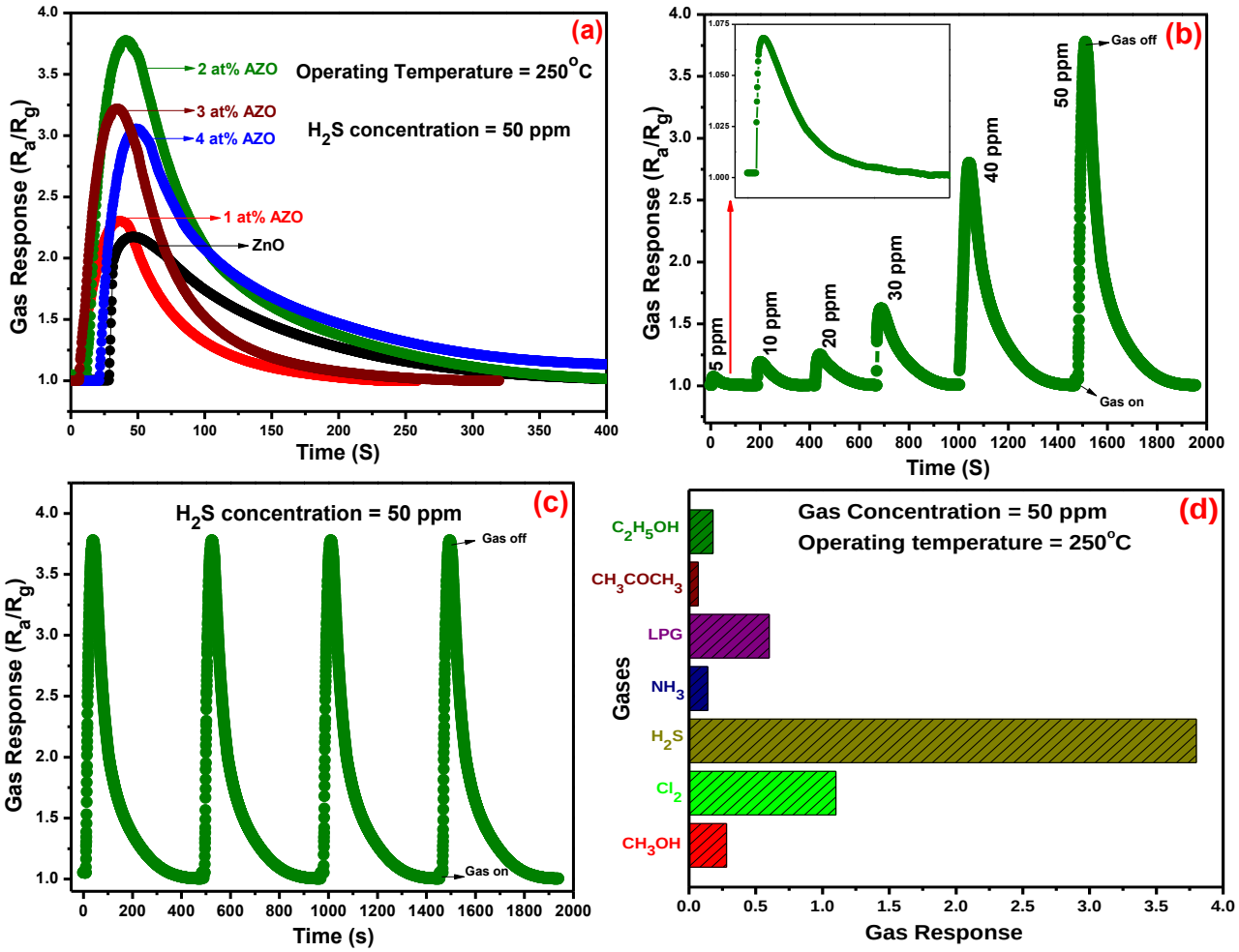
(a)
2 at% AZO
3 at% AZO
4 at% AZO
1 at% AZO
ZnO
Operating Temperature = 250°C
H2S concentration = 50 ppm
Gas Response (Ra/Rg)
Time (S)
(b)
Gas off
Gas on
5 ppm
10 ppm
20 ppm
30 ppm
40 ppm
50 ppm
Gas Response (Ra/Rg)
Time (S)
(c)
H2S concentration = 50 ppm
Gas off
Gas on
Gas Response (Ra/Rg)
Time (s)
(d)
Gas Concentration = 50 ppm
Operating temperature = 250°C
C2H5OH
CH3COCH3
LPG
NH3
H2S
Cl2
CH3OH
Gases
Gas Response

Figure: 4

International e-Conference on Recent Trends in Nano-Materials and Its Applications-2021
In Association withInternational Journal of Scientific Research in Science and Technology
Volume 9 | Issue 2 | Print ISSN: 2395-6011 | Online ISSN: 2395-602X (www.ijsrst.com)

Effect of Particle Size on the Specific Surface Area, Density, and Porosity Of $Mg_{0.8}Zn_{0.2}Cr_xFe_{2-X}O_4$

Swati Patil[1]*, P. M. Kharade[2], J. V. Thombare[3], R.S.Gaikwad[3], S. M. Mane[4], S. S. Dhasade[3]

[1]Department of Physics, Pratapsingh Mohite Mahavidyalaya, Karmala, Dist-Solapur, Maharashtra, India
[2]Department of Physics, Shankarrao Mohite Patil Mahavidyalaya, Akluj, Dist-Solapur, Maharashtra, India
[3]Department of Physics, Vidnyan Mahavidyalaya, Sangola, Dist-Solapur, Maharashtra, India
[4]Department of Physics, Yeungnam University, Gyeongsan,Gyeongbuk 38541, Republic of Korea

ABSTRACT

Particle size optimization is indispensable in many aspects for improving the properties of the materials. Here in nanoparticles of $Mg_{0.8}Zn_{0.2}Cr_xFe_{2-x}O_4$ ferritewere synthesized by the sol-gel auto-combustion method. Through the optimization of various parameters, the dimensions of the nanocrystalline ferrites are achieved within the range of 11- 54 nm. The structural changes with the substitution of Cr were analyzed using X-ray diffraction (XRD). The diffraction pattern confirms the formation of the single-phase spinel structure with cubic symmetry.The effect of particle size on parameters such as specific surface area, density, and porosity are discussed with the help of diffraction patterns. It is observed that replacing Fe^{3+} ions with the Cr^{3+} ions results in enhancement of the nanocrystalline size.

Keywords: Nanocrystalline ferrites; x-ray diffraction; sol-gel method

I. INTRODUCTION

High entropy oxide $(Co,Cr,Fe,Mn,Ni)_3O_4$based spinel structure and its microstructure was studied [1].Single-phase spinel structure nanoferrites of $Mg_{0.8}Zn_{0.2}Cr_xFe_{2-x}O_4$ were prepared by citrate–nitrate auto-combustion methodstructural, humidity sensing,impedance,conductivity and dielectric, properties of Cr^{3+} -substituted Mg–Zn ferrite cubic spinel structure was studied [2-3].Thechanges in structuralandopticalproperties of Mg-doped ZnOnanoparticlesanditsimpactonphotocatalyticefficiencyinalprazolam degradation [4] The fact of decrease in magnetization of ferrite materials is due to the increasing concentration of nonmagnetic Cr^{3+}ions that replaces magnetic Fe^{3+} ions,this results in decreasing thevalue of saturation magnetization of the Mg–Zn ferrite [5].The measured electrical properties of ferrite samples show a compositional dependencefor the AC conductivity and these materials also indicated semiconductingbehavior[6].Grain and grain boundariesof the sample will affect the conductivity of materials, at low-frequency grain boundary resistance and capacitance are contributed while at high frequency grain resistance and capacitance is contributed [7].The cubic spinel structure is maintained for all the samples of Mg-Zn ferrites by doping chromium, the crystal size increases with an

increase in doping materials[8].In the respective systems, the length between the magnetic particles of the constituent ions is decreased by increasing Al^{3+} and Cr^{3+} substitution [9].As the Cr^{3+} substitution for Fe^{3+} increases for Li-based ferrites, it will decrease curie temperature T_C and approaches the compensation temperature T_k [10].Due to the spin disorder in the surface layer of the particles,a decrease of magnetization was observed by increasing Cr doping concentration in lithium ferrite nanoparticles[11].Increasing Cr contents in Co-Fe ferrites will decrease the magnetic hyperfine fields and the Neel temperature, with further increase in the concentration of chromium ions contents size of particle will also decrease [12].Due to the smaller ionic radiiof the doped cation Cr^{3+},the lattice parameter and hence saturation magnetizationof cobalt ferrites decreases with the increase of the Crsubstitution (x) [13].The tetrahedral (A) and octahedral (B) stretching vibrations decrease with increases in Zn concentrations of Mg--Ni-Ferrites [14].TheSingle-phase cubic spinel structure of magnesium ferrite was determined by x-ray diffraction pattern and its hopping length, tetra edge, and octal edge, etc. structural parameters were also determined [15].With increasing Cr concentration in Li ferrite,X-ray density, coercivity,and porosity are increasing whereas particle size bulk density and Lattice parameter, are found to decreaseand alsothe saturation magnetization decreases linearly with increasing Cr^{3+} content[16].The saturation magnetization of lithium ferrite was studied and was found to decreases monotonically with increasing Cr-substitution content, with increasing frequency the real and imaginary parts of permittivity and permeability values decreased gradually [17].Structural and electrical properties of lithium nano ferrites were shown to be a function of composition and temperature[18].Copper doped Lithium Ferrite Nanocompositeshows the paramagnetic behavior and also it is observed that nanocomposites of ferrite exhibit the higher specific capacitance [19].P. Kharbanda et al reported homogeneousness of ferrite magnetic materialand also reported that different grain size distribution, of ferrite materials, is due to thedifference in the growth rate of individual phases in the samples [20].

II. EXPERIMENTAL

Nanocrystalline powders of $Mg_{0.8}Zn_{0.2}Cr_xFe_{2-x}O_4$were prepared by the sol-gelauto-combustion method. The A.R. grade citric acid ($C_6H_8O_7{\cdot}H_2O$), Magnesium nitrate $Mg(NO_3)_2.6H_2O$, Zinc nitrate $Zn(NO_3)_2.6H_2O$, chromium nitrate ($Cr(NO_3)_3{\cdot}9H_2O$) and ferric nitrate$Fe(NO_3)_3{\cdot}9H_2O$ were used as preparatory materials. Synthesis was carried out inthe air atmosphere without protecting by any inert gases. The molar ratio ofmetal nitrates to citric acid was taken as 1:3. The metal nitrates weredissolved together in a minimum amount of double distilled water to get aclear solution. An aqueous solution of citric acid was mixed with metal nitratessolution, then ammonia solution was slowly added to adjust the pH at 7. Themixed solution was kept on a hot plate with continuous stirring at 90 ^{0}C.During evaporation, the solution became viscous and finally formed a veryviscous brown gel. When finally all water molecules were removed from themixture, the viscous gel began frothing. After few minutes, the gelautomatically ignited and burnt with glowing flints. The decompositionreaction would not stop before the entire citrate complex was consumed. Theauto-combustion was completed within a minute, yielding the brown-coloredashes termed as a precursor. Prepared powder was then annealed at 600 ^{0}C for 6 h. Finally, a fine powder with brown color was obtained.

III. RESULTS AND DISCUSSION

X-ray diffraction:

The X-ray diffraction pattern of $Mg_{0.8}Zn_{0.2}Cr_xFe_{2-x}O_4$spinelsis shown in **Figure 1**. All Mg-Zn ferrite

samples show clearXRD reflections from the plains (220), (311), (400),(421), (422), (511), (440), and (533). The formation of the single-phase cubicspinel structure with the Fd3m space groupis in good agreement with JCPDS card number 01-071-1254. Someofthe phasesrelatedtoFe2O4Zn (ref. number 01-073-1963) and Cr2O3(ref. number 01-084-0312) are alsoobservedintheXRDpattern atthehighersubstitutionofCr3+ ions.

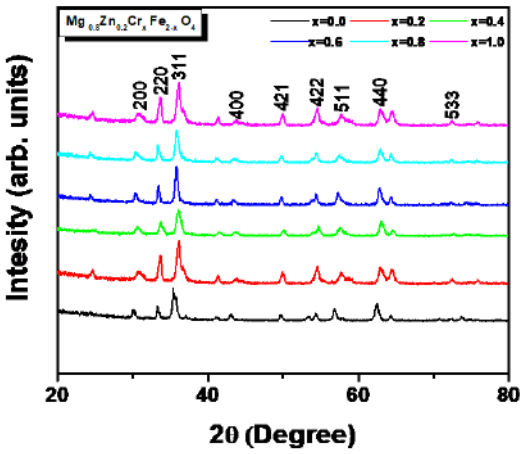

Fig. 1 XRD pattern of $Mg_{0.8}Zn_{0.2}Cr_xFe_{2-x}O_4$

These reflectionsagree quite well with powder reflections of the majority ofthe spinel systems [21]. By indexing the observed reflections of the XRD patterns the parameters of unit cell i.e. lattice constant were determined. The noticeable change in the calculated lattice constant(a) with an increase in Cr substitution is shown in **Table1**.The lattice constant(a) of all the samples was determined by using the following equation [21].

$$a = \frac{\lambda}{2}\left[\frac{\left(h^2+k^2+l^2\right)^2}{\sin\theta}\right] \quad \text{---------- (1)}$$

where ɵ is the angle of diffraction corresponding to the (hkl) plane and (hkl) are the Miller indices.The values of lattice-constant were obtained for every Mg-Zn ferrite sample using XRD data and are shown in **Table 1**. Variation of lattice constant 'a' and X-ray density 'dx' with Cr content x is shown in **Fig.3**.From the figure, it is observed that with an increase in Cr^{3+} content x, the lattice constant decreases. Thedecreaseinthelatticeconstantisrelated tothedifferenceinionicradiiofCr3+and Fe3+.Inthepresent ferrite system Fe3+ions having ionic radii,0.67 A° arereplacedbythe comparatively smallCr3+ ions having ionic radii 0.64 A°. Usingthefollowingexpression the X-ray density 'dX' was calculated

$$dx = \frac{8M}{Na^3} \quad \text{---------- (2)}$$

where 'a' isthelatticeconstant,'M' isthemolecularweightand'N' istheAvogadro's number. From **Table 1**itcanbeseenthat withincreasingtheCr3+content x,theX-ray densitydecreases.Thisdecrease in X-ray density may beduetothedecreaseinmolecularweightof the ferrite sample whichresults in thedecreaseofvolume.Thebroadening in diffractionlinesreflected bytheferritepowderisindicativeofthefineparticlenature oftheferrite.Usingthelinebroadeningofthemostintense (311)diffraction peak,the average crystallite size(t) was determined by usingtheDebyeScherrerformula [21,22].

$$t = \frac{0.9\lambda}{\beta\cos\theta} \quad \text{---------- (3)}$$

where β is thefullwidthathalfmaximumintensity measured inradian,λ is thewavelength, and ɵ is theBraggangle.**Table 1** shows thevariationofthecrystallite sizewithCrcontentx. Thecrystallitesize of ferrite powder increasedfrom10.91nmto 54.46nmwithincreasingCrcontent x.The above resultindicatesthattheaveragecrystallitesizeoftheferrite powdersismuch moredependentonthechromiumion concentrationandincreases withan increase in Cr ions,whichindicatesthatthe grain growth of ferrite powder is promoted by theadditionofchromium ion.**Fig. (2a)** and **(2b)** are the transmission electron micrographs (TEM) of x=0.8 and 1.0,respectively.It is evident from the graphs that all the synthesized particles do not have a specific shape.Both the figures confirm that most of the particles are of size about

10–54 nm. This is in close agreement with the average crystallite size obtained from XRD (**Table 1**).

Table 1

Lattice constant (a), X-ray density (dx), particle size (t),specific surface area(s),bulk density (d_B), and porosity(P) of $Mg_{0.8}Zn_{0.2}Cr_xFe_{2-x}O_4$

Comp. X	a (A^0)	dx (A^0)	t nm	s m^2/gm	d_B gm/cm^3	P %
0.0	8.381	4.6987	10.91	108.91	3.9177	16.62
0.2	8.375	4.6919	18.17	65.35	3.9777	15.22
0.4	8.368	4.6862	26.45	44.92	4.0132	14.36
0.6	8.360	4.6822	27.26	43.58	4.0463	13.58
0.8	8.355	4.6730	27.27	43.56	4.0930	12.41
1.0	8.348	4.6670	54.46	21.81	4.1218	11.68

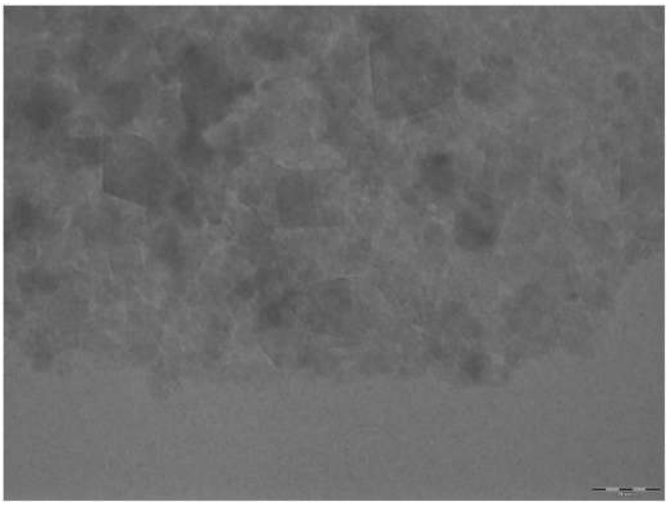

Fig. (2a) TEM image of $Mg_{0.8}Zn_{0.2}Cr_xFe_{2-x}O_4$ with X=0.8

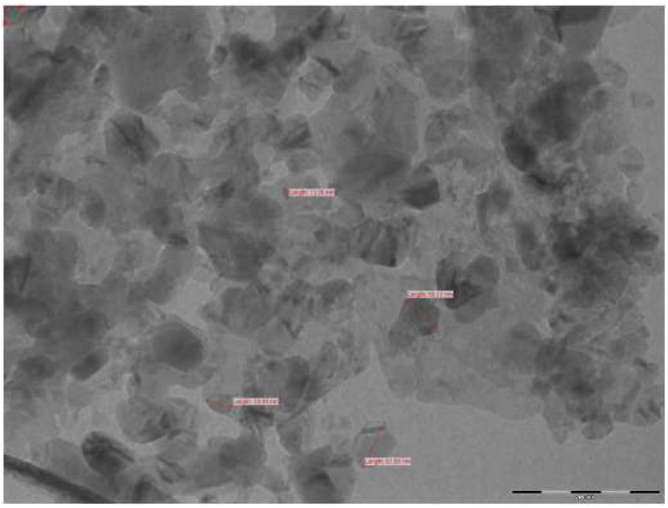

Fig. (2b) TEM image of $Mg_{0.8}Zn_{0.2}Cr_xFe_{2-x}O_4$ with X=1.0

From the diameter of the particle(D) in nanometers anddensity of the particle (ρ) the specificsurfacearea(S) was calculated using the following relation [23].

$$s = \frac{6000}{D\rho} \quad \text{---------- (4)}$$

Table 1.shows the valuesofsurfacearea. **Fig.3** shows that withincreasing Cr^{3+} content, the specific surface area decreases. Duetotheincreaseincrystallitesizeof ferrite powder thespecific surface area S decreases.

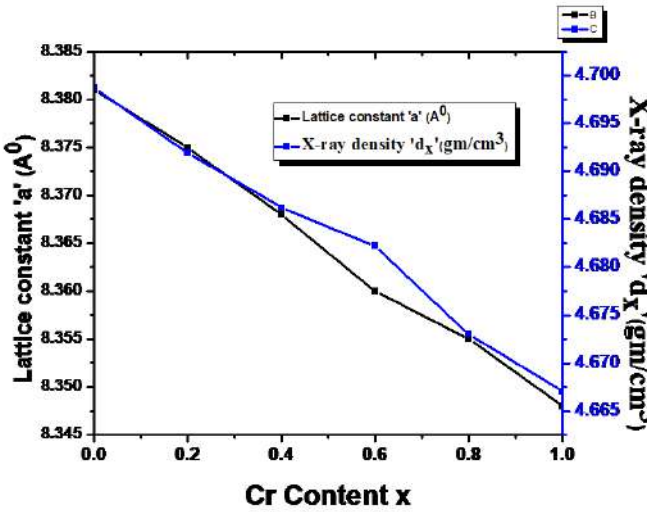

Fig.3 Variation of lattice constant 'a' and X-ray density 'dx' with Cr content x.

Byusing theArchimedes'methodthebulkdensity'dB'of thespecimenswasdetermined.The valuesofthebulkdensityareshownin **Table 1.** WithincreasingCrcontent x,thebulkdensity of ferrite

powder wasfoundtoincrease. **Fig.4** shows the variation of bulk density 'dB' and Porosity 'P' with Cr content x.

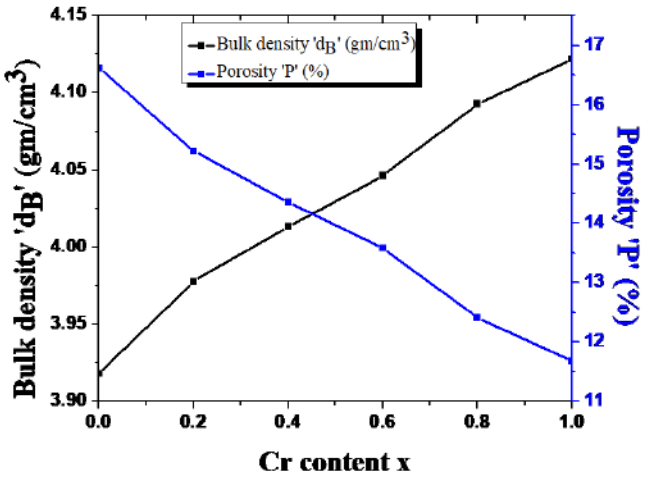

Fig.4 Variation of bulk density 'dB' and Porosity 'P' with Cr content x

Theporosity 'P' oftheferritenanoparticlescanbedeterminedusingthe followingrelation [24].

$$p = 1 - \frac{dB}{dx} \quad \text{---------- (5)}$$

IV. CONCLUSION

NanocrystallineMg-Zn ferrite powder particles are successfully synthesized by a simple sol-gel auto combustion method.The Single-phase formation of spinel structure with cubic symmetry was confirmed by XRD. The effect of particle size on parameters such as specific surface area, density, and porosity isstudied.The result indicates that the average crystallite size of the ferrite powders is much more dependent on the chromium ion concentration.With the increase in Cr^{3+} content x, the lattice constant decreases. The decrease in the lattice constant is related to the difference in ionic radii of $Cr^{3+}$and Fe^{3+}. In the present ferrite system Fe^{3+}ions having ionic radii, 0.67 A˚ are replaced by the comparatively small Cr3+ ions having ionic radii 0.64 A˚.

V. REFERENCES

[1]. Synthesis and microstructure of the (Co,Cr,Fe,Mn,Ni)3O4 high entropy oxide characterized by spinel structure,JuliuszDąbrowa, MirosławStygar, Andrzej Mikuła, Arkadiusz Knapik, Krzysztof Mroczka, Waldemar Tejchman, Marek Danielewski, Manfred Martin,Materials Letters ,216 (2018) 32-36

[2]. Improvement of physico-mechanical properties of Mg–Zn nanoferrites via Cr3+ doping,S.F. Mansour, M.A. Abdo, S.I. El-Dek,Journal of Magnetism and Magnetic Materials,422 (2017) 105-111

[3]. Synthesis and investigation of structural, dielectric, impedance,conductivity and humidity sensing properties of Cr3+-substituted Mg–Zn ferrite nanoparticle, TugbaSasmaz Kuru,Applied Physics A, 126 (2020) 419

[4]. Effect of annealing temperature on structural and optical properties of Mg-doped ZnO nanoparticles and their photocatalytic efficiency in alprazolam degradation, T.B. Ivetic, M.R.Dimitrievska, N.L.Finčur, Lj.R. Đačanin, I.O.Gúth, B.F. Abramović, S.R.Lukić-Petrović,Ceramics International, 40 (2014) 1545-1552

[5]. S.J. Haralkar, R.H.Kadam , S.SMore, SagarE.Shirsath, M.L.Mane, SwatiPatil, D.R.Mane,Substitutional effectofCr3+ ions on the properties of Mg–Zn ferrite nanoparticles,Physica B,407 (2012) 4338–4346

[6]. Structural and electromagnetic studies of Mg1-xZnxFe2O4nanoparticles synthesized via a sucrose auto combustion route,M. A. Gabal, A. A. Al-Juaid,Journal of Materials Science: Materials in Electronics,31, (2020),10055–10071

[7]. Dielectric, magnetic and humidity properties of MgeZneCr ferrites,Mehmet Kuru, TugbaSasmaz Kuru, ErtugrulKaraca, SadıkBagc,Journal of Alloys and Compounds 836 (2020) 155318

[8]. Improvement of physico-mechanical properties of mg-znnanoferrites via cr3+ doping,Journal of Magnetism and Magnetic Materials, 422 (2017) 105-111

[9]. Ion Jump Lengths Of MN-ZN-AL-FE And MG-ZN-CR-FE Nano-particles,S. J. Haralkar, S. S. More, Sagar E. Shirsath, R. H. Kadam, D. R. Mane,Indian Streams Research Journal,2 (2012) 1-6

[10]. On the magnetic compensation effect of lithium-chromium ferrites Li0.5CrxFe2.5–xO4 ($0 \le x \le 1.55$) A. Rais, A. M. Gismelseed, and I. A. Al-Omar,Phys. stat. sol. (b) 242, No. 14, (2005) 2949–2955

[11]. Effect of chromium substituted on structural and magnetic characterization lithium ferrite nanoparticles,Nguyen Thi Lan, Phuong Dinh Tam, Nguyen Phuong Duong, Than Duc Hien,Vietnam Journal of Chemistry, International Edition, 55(4) (2017) 521-526

[12]. Crystallographic and magnetic properties of CoCrxFe2˜xO4 ferrite powders, Kwang Pyo Chae, Young Bae Lee, Jae Gwang Lee, Sung-Ho Lee,Journal of Magnetism and Magnetic Materials 220 (2000) 59-64

[13]. The Effect of Cr3+ Substitution on Magnetic Properties of CoFe2O4 Nanoparticles Synthesized by Microwave Combustion Route, A. Baykal, S.Eryigit, M. Sertko, S. Unlu A. Yildiz, Sagar E. Shirsath,J Supercond Nov Magn, 2400 (2016) 29:2395

[14]. Effects of Zn Substitution on Structure Factors,Debye-Waller Factors and Related Structural Properties of the Mg1-xZnxFeNiO4Spinels,Kadhim Ahmed Khalaf, Ahmed Al-Rawas, AbbasherGismelseed, Majid Al-Ruqeishi,Salwan Al-Ani, Ahmad Al-Jubouri, Khamis Al-Ryami, Bushra Al-Jaddedi,Advances in Materials, 8(2) (2019) 70-93

[15]. Low-temperature synthesis, structural characteristic of magnesium ferrite Vinay Mahale, A V Raut, V K Surashe,S. R.Nimbhore, R G Dorik and D R Shengule,Journal of Physics: Conference Series 1644 (2020) 012013

[16]. Sol-gel synthesis of Cr3+ substituted Li0.5Fe2.5O4: Cation distribution, structural and magnetic properties, D.R. Mane, Swati Patil, D.D. Birajdar, A.B. Kadam, Sagar E. Shirsathc, R.H. Kadam,Materials Chemistry and Physics 126 (2011) 755–760

[17]. Microwave properties of chromium-substituted lithium ferrite,Yen-Pei Fu,Dung-Shing Hung,Yeong-Der Yao, Ceramics International 35 (2009) 2179–2184

[18]. Electrical Conductivity and Magnetic Properties Studies of Chromium Substituted Lithium Nano Ferrites, D. Ravinder Nayak,Poornima. B. Shetty, D. Ravinder,International Journal of Latest Technology in Engineering, Management & Applied Science 7 (2018) 2278-2540

[19]. Synthesis and Characterization of Copper Doped Lithium Ferrite Nanocomposite,P. Hajasharif, K.Ramesh, S.Sivakumar,P. Sivagurunathan,International Journal of Innovative Technology and Exploring Engineering 9 (2019) 33-37

[20]. Ferrites: magnetic materials asan alternate source of green electrical energy,Pranati Kharbanda, Tushar Madaan, Isha Sharma, Shruti Vashishtha,Parveen Kumar, Arti Chauhan, Sumit Mittal, Jarnail S. Bangruwa,Vivek Verma,.heliyon.(2019) 01151 (https://doi.org/10.1016/j.heliyon.2019.e01151)

[21]. M.V.Kuznetsov,Q.A.Pankhurst,I.P.Parkin,J.Mater.Chem.8(1998)2701.

[22]. Substitutional effect of Cr3+ ions on the properties of Mg–Zn ferrite nanoparticles,S.J. Haralkar, R.H.Kadam, S.S More, Sagar E.Shirsath, M.L.Mane, Swati Patil, D.R.Mane,Physica B 407 (2012) 4338–4346

[23]. M.George,A.M.John,S.S.Nair,P.A.Joy,M.R.Anantharaman,J.Magn.Magn.Mater. 302(2006)190.

[24]. S.M.Patange,SagarE.Shirsath,B.G.Toksha,S.S.Jadhav,K.M.Jadhav,J.Appl.Phys. 106(2009)023914

International e-Conference on Recent Trends in Nano-Materials and Its Applications-2021
In Association with International Journal of Scientific Research in Science and Technology
Volume 9 | Issue 2 | Print ISSN: 2395-6011 | Online ISSN: 2395-602X (www.ijsrst.com)

FTIR and VSM Study of Sol-Gel Synthesized Nanoparticles Of $Mg_{0.8}Zn_{0.2}Cr_xFe_{2-x}O_4$

Swati Patil[1]*, P. M. Kharade[2], J. V. Thombare[3], R.S.Gaikwad[3], Sagar Mane[4], S. S. Dhasade[3]

[1]Department of Physics, Pratapsingh Mohite Mahavidyalaya, Karmala, Dist-Solapur, Maharashtra, India
[2]Department of Physics, Shankarrao Mohite Patil Mahavidyalaya, Akluj, Dist-Solapur, Maharashtra, India
[3]Department of Physics, Vidnyan Mahavidyalaya, Sangola, Dist-Solapur, Maharashtra, India
[4]Department of Physics, Yeungnam University, Gyeongsan, Gyeongbuk 38541, Republic of Korea

ABSTRACT

In this study, spinel magnesium zinc ferrite ($Mg_{0.8}Zn_{0.2}Cr_xFe_{2-x}O_4$: x = 0.0, 0.2, 0.4, 0.6, 0.8 and 1.0) nanoparticles were synthesized by sol-gel auto combustion method. The effects of chromium ions on the functional group and magnetic properties of spinel Mg-Zn ferrites nanocomposites were investigated. Characterization methods such as Fourier transform infrared (FT-IR) spectroscopy and vibrating sample magnetometer (VSM) were used to study functional group determination and magnetic properties of ferrite materials. With the help of FTIR, the nanoregime effect on parameters such as vibration frequency, bond length, and force constant is estimated. Using the Vibrating Sample Magnetometer (VSM), the M–H loop of $Mg_{0.8}Zn_{0.2}Cr_xFe_{2-x}O_4$ has been traced and saturation magnetization (M_s), coercivity (H_C), and retentivity (M_R) studied.

Keywords: Mg-Zn ferrites; sol-gel synthesis; FTIR; VSM.

I. INTRODUCTION

Doping of Sm and Co in bismuth ferrite will influence the properties like magnetic, structural, dielectric, ferroelectric, and leakage current density [1]. Spinel structure formation and cation distribution of ferrite powder are confirmed by using Fourier transform infrared spectroscopy with the proposed data using XRD [2]. The ability of nanoporous ferrite to dissociate water molecules has been exploited to develop a green electrical energy cell, which is a combination of electrode chemistry and material science [3]. Lithium-nickel ferrite nanocrystalline particles were synthesized by a low-temperature citrate gel auto combustion method and its structural parameters like lattice parameter, X-ray density, bulk density, and porosity has determined [4] Magnetization Mg-doped lithium ferrite decreases with increases in doping percentage of magnesium and it vanishes above the comparatively high Curie temperature Tc of 900 K [5]. By using the laser diffraction technique the dispersity of the synthesized lithium ferrite powder was investigated, it is seen that there are slight decreases in the average particle size of the ferrite powder by an increase in the mechanical milling time [6]. Copper-doped cobalt ferrite

nanoparticles show a decrease in crystallite size with an increase in doping materials, while VSM results showed that the final materials are ferromagnetic and there is a decrease in magnetization due to the decrease in the value of magnetic moments of octahedral sites[7]. Cobalt doped spinel $MgFe_2O_4$ ferrite nanocomposites with improved magneto-optical and photocatalytic properties of transition metal are seen, as cobalt content increases bandgap of ferrite material goes on increases [8]. Dye-sensitized solar cell based on FeO nanorods shows conversion efficiency of 0.43%, under the light radiation of 1000 W/m^2, which is enhanced than FeO nanoparticles [9] By increasing heating rate, the average crystallite size of sintered ferrite samples decreases, during the heating period the specific surface of nanosized Mn-Zn ferrite powder strongly enhances while the density of ferrite decrease [10] The coordinates of atoms, the dimensions of the unit cell, the occupation factors of the atom, isotropic temperature factors, as well as the interatomic distances of copper doped Mg-Zn ferrite have been determined.[11] The dielectric constant of prepared spinel ferrites decreases gradually as the concentration of rare-earth ions increases in the ferrites, this is due to the exchange of electrons between Fe^{2+} and Fe^{3+} [12] By controlling the size and composition, contrast agents of Iron oxide has been developed as T_1 or T_2 for magnetic resonance imaging (MRI), they show significant interactional T_1 and T_2 contrast effects [13] Multi ferroic samples of bismuth ferrite shows the change of rhombohedral structure to a tetragonal structure after doping of Sm and CO, further it shows an increase in the symmetry and decrease in phases, Furthermore, the dielectric properties bismuth ferrites enhance with co-doping.[14] To fabricate a magnetite-based Hydroelectric Cell a chemical method is used to synthesis mesoporous magnetite nanoparticles and its ionic diffusion of dissociated ions has been confirmed, furthermore, it is observed that due to less Ohmic loss in magnetite cell current increases [15] Mn-Zn ferrite was synthesized by simple one-pot microwave combustion method, it was observed that the magnetization values of Mn-Zn ferrites increased with increasing Mn^{2+} cation, this increased values of magnetization is due to the replacement of Zn^{2+} by Mn^{2+} in the $ZnFe_2O_4$ lattice and also due to the distribution of cations at tetrahedral and octahedral sites [16] By solution combustion method single phase Cobalt copper ferrite nanopowders with increased particle size were synthesized, with an increase of Cu^{2+} ions concentration in cobalt ferrite X-ray density increase due to increase in electron density [17]

II. EXPERIMENTAL

Nanocrystalline powders of Mg 0.8Zn0.2 Crx Fe2-x O4 were prepared by the sol-gel auto-combustion method. The A.R. grade citric acid (C6H8O7·H2O), Magnesium nitrate Mg(NO3)2.6H2O, Zinc nitrate $Zn(NO_3)_2$.6H2O, chromium nitrate (Cr(NO3)3·9H2O) and ferric nitrate Fe(NO3)3·9H2O were used as preparatory materials. Synthesis was carried out in the air atmosphere without protecting by any inert gases. The molar ratio of metal nitrates to citric acid was taken as 1:3. The metal nitrates were dissolved together in a minimum amount of double distilled water to get a clear solution. An aqueous solution of citric acid was mixed with metal nitrates solution, then ammonia solution was slowly added to adjust the pH at 7. The mixed solution was kept on a hot plate with continuous stirring at 90 °C. During evaporation, the solution became viscous and finally formed a very viscous brown gel. When finally all water molecules were removed from the mixture, the viscous gel began frothing. After few minutes, the gel automatically ignited and burnt with glowing flints. The decomposition reaction would not stop before the entire citrate complex was consumed. The auto-combustion was completed within a minute, yielding the brown-colored ashes termed as a precursor. Prepared powder was then annealed at 600 ^{0}C for 6h. finally, a fine powder with brown color was obtained.

III. RESULTS AND DISCUSSION

FTIR spectroscopy:

Fig. 1 shows the FTIR spectrum of as-synthesized powder of $Mg_{0.8}Zn_{0.2}Cr_xFe_{2-x}O_4$ in the frequency range of 800–400. The positions of the ions in the crystal through the vibrational modes of a crystal can be studied with the help of an infrared absorption spectrum. It is known that the normal cubic spinels have two IR bands representing the fundamental absorption bands.

From **Fig. 1** and **Table 1** it is observed that there are two main frequency bands, namely, the high frequency band(υ_1) is observed at 529-549 cm^{-1} whereas the lower frequency band (υ_2) is observed at 422–466 cm^{-1}. The intensity of the high frequency band(υ_1) and frequency band(υ_2) appears to increase with the addition of Cr^{3+} ions. These two observed frequency bands υ_1 and υ_2 are the characteristics of all the ferrite composites and they correspond to the intrinsic vibrations of tetrahedral and octahedral $Fe^{3+}-O_2^{2-}$ complexes, respectively. It explains that the normal mode of vibration of the octahedral cluster is lower than that of the tetrahedral cluster. From FTIR data it is seen that the normal mode of vibration of the tetrahedral cluster (529 cm^{-1}) is higher than that of the octahedral cluster (422 cm^{-1}). This can be due to the long bond length of an octahedral cluster than the tetrahedral cluster[18]. This presence of a long shoulder for the A-site is indicative of the presence of other ionic states in that site. By increasing the Cr^{3+} content in ferrite powder, the vibrational frequencies $\upsilon 1$ and $\upsilon 2$ of all the compositions change. Due to the changes in bond lengths $Fe^{3+}-O_2^{2-}$ within octahedral and tetrahedral sites, the difference in frequencies between $\upsilon 1$and $\upsilon 2$ is observed. The metal-oxygen vibrational energies increases due to the decrease in the $Fe_B^{3+}-O_2^{2-}$ intermolecular distance, which arises from the increase of the number of $Cr^{3+}-O_2^{2-}$ complexes caused by the decrease in the number of $Fe^{3+}-O_2^{2-}$ complexes and the formation of Mg^{2+}/Zn^{2+} [19].

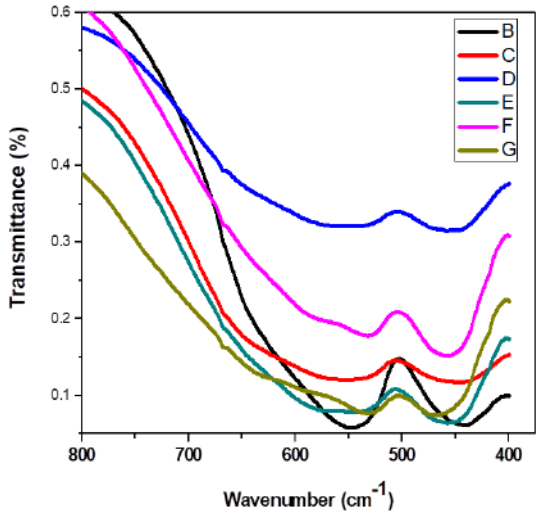

Fig.1 The FTIR spectrum of as-synthesized powder of $Mg_{0.8}Zn_{0.2}Cr_xFe_{2-x}O_4$

Comp. x	υ_1 (cm^{-1})	υ_2 (cm^{-1})	K_O x 10^4 (dyne/cm)	K_t x 10^4 (dyne/cm)
0.0	529	422	9.7603	8.5091
0.2	532	443	10.8399	8.6814
0.4	539	457	11.2090	8.6919
0.6	540	458	11.4719	8.7496
0.8	546	465	11.7285	8.8317
1.0	549	466	11.7445	8.8848

Table.1 Band position ($\nu_1$and ν_2), force constant (K_O and K_t) of $Mg_{0.8}Zn_{0.2}Cr_xFe_{2-x}O_4$.

The increasing force constant and shortening of metal-oxygen bonds of the octahedral unit is attributed to the increase in vibrational frequency (υ_2) with an increase in Cr^{3+} content in ferrite material. The force constant is the second derivative of the potential energy concerning the site radius with the other independent parameters kept constant. The force constant for the octahedral site(K_O) and tetrahedral site(K_t) were calculated by employing the Waldron method [20]. According to Waldron the

force constant K_t and K_O for respective sites are given by

$$K_t = 7.62 M_1 \nu_1^2 x10^{-3} \text{ dynes/cm} \text{----------(1)}$$

$$K_o = 10.62 \frac{M_2}{2} \nu_1^2 x10^{-3} \text{ dynes/cm} \text{----------(2)}$$

where M1 and M2 are the molecular weight of cations on the A and B sites respectively.

IV. MAGNETIC STUDIES

Substitution of Cr^{3+} ions into magnesium ferrite significantly affects the magnetic properties of ferrite materials. **Fig. 2** shows the plots of hysteresis loops for $Mg_{0.8}Zn_{0.2}Cr_xFe_{2-x}O_4$ samples. This **Fig.2** indicates that the magnesium ferrite is a soft magnetic material, which revealed minimal hysteresis. The shape and the width of the hysteresis loop depend on factors such as the porosity, grain size, and chemical composition of the compound, etc. From the field dependence of magnetization, ferrimagnetic behavior for all the samples has been observed.

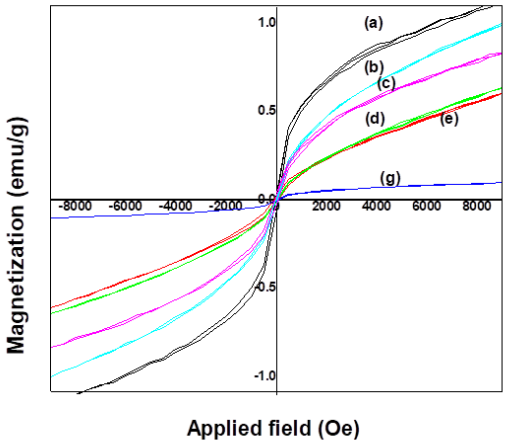

Fig. 2 Variation of magnetization with applied field measured at 300K,(a) x= 0.0, (b) x=0.2, (c) x= 0.4, (d) x=0.6, (e) x= 0.8 and(f) x= 1.0 of $Mg_{0.8}Zn_{0.2}Cr_xFe_{2-x}O_4$

From these magnetization curves (**Fig. 2**) the observed magnetic moment per formula unit,($M_{obs.}$) was determined, by extrapolating the high-field part of the curves to zero fields. In a spinel ferrite, each ion at the A site has 12 B-site ions as nearest neighbors. According to Neel's molecular field model [21], the A–B superexchange interactions dominate the intra sublattice A–A and B–B interactions. The difference of the magnetic moments of the A and B sublattices gives the net magnetic moment.[20,22]

The coercivity field, H_C reflects the coercivity for a ferromagnetic or ferrimagnetic material. This value of coercivity refers to the strength of the magnetic field required to reduce the magnetization of the ferrite magnetic sample to zero after the magnetization of the ferrite sample has reached saturation. The coercivity was observed to be significantly affected by Cr^{3+} substitution in the magnesium ferrite. It can be seen from **Fig. 3** and **Table. 2** that the coercivity increases with increasing Cr^{3+} content. According to the one-ion model, the anisotropy field in the ferrites depends on the amount of sum of effects of the different magnetic ions [23]. Values of saturation magnetization(Ms) and coercivity determined from hysteresis loops are presented in **Table 2.**

Comp. x	Ms (emu/g)	Hc (Oe)
0.0	1.1454	16.24
0.2	1.001	41.46
0.4	0.833	44.88
0.6	0.6415	56.95
0.8	0.608	61.57
1.0	0.1003	88.34

Table.2 Shows the values of magnetization(Ms), coercivity (Hc), of $Mg_{0.8}Zn_{0.2}Cr_xFe_{2-x}O_4$ with composition

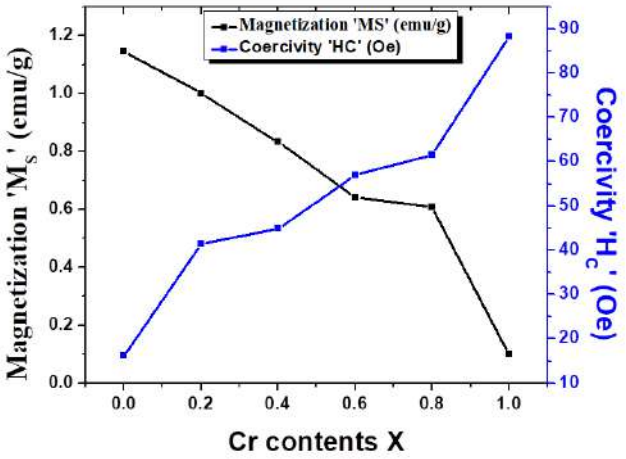

Fig. 3. Variation of saturation magnetization(M_s) and coercivity (H_C) with Cr content x.

V. CONCLUSION

The Infra-Red analysis supports the currently accepted cation distribution. With the increasing Cr^{3+} (x) content in ferrite materials, the saturation magnetization decreases linearly. The decrease in saturation magnetization is attributed to the fact that the increasing concentration of nonmagnetic Cr^{3+} ions. These nonmagnetic Cr^{3+} ions replace magnetic Fe^{3+} ions results in decreasing the value of saturation magnetization of the Mg–Zn ferrite.

VI. REFERENCES

[1]. Modified ferroelectric/magnetic and leakage current density properties of Co and Sm co-doped bismuth ferrites, Balesh Kumar Vashisth, Jarnail S. Bangruwa, Anu Beniwal, S.P. Gairola, Ashok Kumar, Nidhi Singh, Vivek VermaJournal of Alloys and Compounds, 698 (2017) 699-705

[2]. Sol-gel route of synthesis of nanoparticles of Mg Fe2O4 and XRD, FTIR and VSM study, A. Pradeep, P. Priyadharsini, G. Chandrasekaran, Journal of Magnetism and Magnetic Materials 320 (2008) 2774– 2779

[3]. Green hydroelectrical energy source based on water dissociation by nanoporous ferrite Ravinder Kumar Kotnala, and Jyoti Shah, Int. J. Energy Res. 40 (2016) 1652-1661

[4]. Structural and Electrical Properties of Li–Ni Nanoferrites Synthesised by Citrate Gel Autocombustion Method, G. Aravind, D. Ravinder, and V. Nathanial, Physics Research International, Volume 2014, Article ID 672739, 11 pages

[5]. Magnetic study of nanocrystalline Mg-doped lithium ferrite, Marek Pekala, Frank J. Berry, Hisham M Widatallah, Czechoslovak Journal of Physics, 52 (2002) 101-104

[6]. Influence of mechanical milling conditions on the dispersity of lithium ferrite, S A Lamonova, E N Lysenko and A V Malyshev, Materials Science and Engineering 93 (2015) 012035

[7]. Structural characterization and magnetic properties of undoped and copper-doped cobalt ferrite nanoparticles prepared by the octanoate coprecipitation route at very low dopant concentrations, Hypolite Mathias Kamta Tedjieukeng, Patrice Kenfack Tsobnang, Roussin Lontio Fomekong, Ekane Peter Etape, Pattayil A. Joy, Arnaud Delcortee and John Ngolui Lambia, Royal Society of Chemistry, 8 (2018) 38621–38630

[8]. Enhanced magneto-optical and photocatalytic properties of transition metal cobalt (Co2+ ions) doped spinel MgFe2O4 ferrite nanocomposites, A. Godlyn Abraham, A. Manikandan, E. Manikandan, S. Vadivel, S.K. Jaganathan, A. Baykal, P. Sri Renganathan, Journal of Magnetism and Magnetic Materials, 452 (2018) 380-388

[9]. One-Pot Low Temperature Synthesis and Characterization Studies of Nanocrystalline α-Fe2O3 Based Dye Sensitized Solar Cells, A. Manikandan, A. Saravanan, S. Arul Antony, and M. Bououdina, Journal of Nanoscience and Nanotechnology, 15 (2015) 4358–4366

[10]. Sintering of Nanosized Mn-Zn Ferrite Powders, Marko Rozman and Miha Drofenik, American Ceramic Society, 81(1998) 1757–64

[11]. Application of Rietveld Method to the Structural Characteristics of Substituted Copper Ferrite Compounds, S. Ahmed Farag, M. A. Ahmed, S. M. Hammad, A. M. Moustafa, Cryst. Res. Technol., 36 (2001) 85–92

[12]. Structural and dielectric properties of copper-based spinel ferrites, The European Physical Journal Plus, Hafiz Muhammad Tahir Farid,Ishtiaq Ahmad, Irshad Ali, Asif Mahmood, and Shahid M. Ramay, 41 (2018) 133

[13]. Interplay between Longitudinal and Transverse Contrasts in Fe3O4 Nanoplates with (111) Exposed Surfaces, Zijian Zhou,Zhenghuan Zhao,Hui Zhang,Zhenyu Wang, Xiaoyuan Chen, Ruifang Wang,Zhong Chen, and Jinhao Gao, ACS anao, 8 (2014) 7976–7985

[14]. Modified ferroelectric/magnetic and leakage current density properties of Co and Sm co-doped bismuth ferrites, Balesh Kumar Vashisth1, Jarnail S. Bangruwa, Anu Beniwal, S.P. Gairola, Ashok Kumar, Nidhi Singh, Vivek Verma, Modified ferroelectric/magnetic and leakage current density properties of Co and Sm co-doped bismuth ferrites, Journal of Alloys and Compounds, 698, (2017) 699-705

[15]. Environment-Friendly Mesoporous Magnetite Nanoparticles-Based Hydroelectric Cell Shipra Jain, Jyoti Shah, S. R. Dhakate, Govind Gupta, C. Sharma, and R. K. Kotnala, J. Phys. Chem. C, 122 (2018) 5908–5916

[16]. Enhanced Catalytic Activity and Magnetic Properties of Spinel MnxZn1–xFe2O4 ($0.0 \leq x \leq 1.0$) Nano-Photocatalysts by Microwave Irradiation Route,G. Padmapriya, A. Manikandan, V. Krishnasamy, Saravana Kumar Jaganathan, S. Arul Antony, Journal of Superconductivity and Novel Magnetism, 29(2016) 8-16

[17]. Role of Cu2+ ions substitution in magnetic and conductivity behaviour of nano CoFe2O4, D.M. Jnaneshwara, D.N. Avadhani, B. Daruka Prasad, H. Nagabhushana,B. M. Nagabhushana, S.C. Sharma, S. C. Prashantha, C. Shivakumaraha, Spectrochimica Acta Part A: Molecular and Biomolecular Spectroscopy, 132 (2014) 256-262

[18]. R.D.Waldron,Phy.Rev.99(1955)1727

[19]. O.Hemeda,M.A.Amer,S.AboulEnein,M.A.Ahmed,Phys.StatusSolidiA156 (1996) 29.

[20]. R.D.Waldron,Phy.Rev.99(1955)1727

[21]. L. Neel, Ann. Phys. 3 (1948) 137

[22]. L. Neel, C.R.Acad.,Sci.Paris230(1950)375

[23]. S.Chikazumi, S.Charap, Physics of Magnetism, John Wiley & Sons, NewYork,1964. (pp.153).